Lessons from combined experimental and theoretical examination of the FTIR and 2D-IR spectroelectrochemistry of the amide I region of cytochrome c

Youssef El Khoury, Guillaume Le Breton, Ana. V. Cunha, Thomas L. C. Jansen, Luuk J. G. W. van Wilderen, Jens Bredenbeck

Lessons from combined experimental and theoretical examination of the FTIR and 2D-IR spectroelectrochemistry of the amide I region of cytochrome *c*

Youssef El Khoury*[a,b], Guillaume Le Breton[c,d], Ana. V. Cunha[c,e], Thomas L. C. Jansen*[c], Luuk J. G. W. van Wilderen[a] and Jens Bredenbeck*[a]

[a] *Institut für Biophysik, Johann-Wolfgang-Goethe-Universität, Max-von-Laue-Strasse. 1, 60438 Frankfurt am Main, Germany.*

Email: bredenbeck@biophysik.org

[b] *Present address: Laboratoire de biolélectrochimie et spectroscopie. 4, Rue Blaise Pascal 67000 Strasbourg, France.*

Email: elkhoury@unistra.fr

[c] *University of Groningen, Zernike Institute for Advanced Materials, Nijenborgh 4, 9747 AG Groningen, The Netherlands.*

Email: t.l.c.jansen@rug.nl

[d] *Present address: Département de Physique, École Normale Supérieure de Lyon, 46 Allée d'Italie, Lyon Cedex 07, France.*

[e] *Present address: Oak Ridge National Laboratory 1 Bethel Valley Road, Oak Ridge, TN 37831, Tennessee, United States of America.*

Abstract

Amide I difference spectroscopy is widely used to investigate protein function and structure changes. In this contribution, we show that the common approach of assigning features in amide I difference signals to distinct secondary structure elements in many cases may not be justified. Evidence comes from FTIR and 2D-IR spectroelectrochemistry of the protein cytochrome *c* in the amide I range, in combination with computational spectroscopy based on molecular dynamics (MD) simulations. This combination reveals that each secondary structure unit, such as an alpha-helix or a beta-sheet, exhibits broad overlapping contributions, usually spanning a large part of the amide I region, which in the case of difference absorption experiments (such as in FTIR spectroelectrochemistry) may lead to intensity-compensating and even sign-changing contributions. We use cytochrome *c* as test case, as this small electron-transferring redox-active protein contains different kinds of secondary structure units. Upon switching its redox-state, the protein exhibits a different charge distribution while largely retaining its structural scaffold. Our theoretical analysis suggests that the change of charge distribution contributes to the spectral changes and that structural changes are small. However, in order to confidently interpret FTIR amide I difference signals in cytochrome *c* and proteins in general, MD simulations in combination with additional experimental approaches such as isotope labeling, the insertion of infrared labels to selectively probe local structural elements will

be required. In case these data are not available, a critical assessment of previous interpretations of protein amide I 1D and 2D-IR difference spectroscopy data is warranted.

I. Introduction

Redox-induced Fourier transform infrared (FTIR)[1] difference spectroscopy has been extremely successful in studying redox-induced changes in proteins and distilling out subtle changes from congested absorption spectra.[2, 3] It found especially widespread use in the analysis and interpretation of the amide I band in proteins, where different secondary structure elements are thought to correlate with distinct spectral domains of the amide I band.[4-12]

2D-IR spectroscopy has been used before to study peptides and proteins,[13-18] and connections between a protein's secondary structure and its 2D-IR spectrum in the amide I region have been demonstrated.[19]

The additional dimension of 2D-IR potentially allows to disentangle complex spectra produced by linear IR spectroscopy. Furthermore, 2D-IR is sensitive to couplings and correlations of vibrations and may thus provide insight into structure changes.

Motivated by the structure-resolving power of two-dimensional infrared (2D-IR) spectroscopy,[20] we performed electrochemically-induced

difference absorption spectroscopy and 2D-IR spectroscopy[21, 22] on horse heart cytochrome *c* (cyt *c*), which is one of the proteins studied in most detail by redox-induced FTIR difference spectroscopy,[23-26] in the amide I range, and attempt to analyse the spectra via commonly-accepted literature assignments linking the amide I absorption band and the different secondary structure elements in the protein.

Cyt *c* is a small water-soluble protein shuttling electrons between the respiratory complexes III and IV. It has a type-*c* heme that is covalently bound to the protein backbone via two Cys residues where the axial positions of the central iron atom are occupied by His18 and Met80.[27] Besides its importance in cellular respiration and photosynthesis, cyt *c* attracts major attention because of its possible role in apoptosis.[28] As a result, cyt *c* has become a widely studied protein where solution[29-31] and crystal structures[27, 32, 33] of cyt *c* from different species in both the Ox and Red states are now available. Based on recent X-ray crystallographic studies,[33] cyt *c* seems to almost completely maintain its secondary structure upon electron transfer. Both solution and crystal structures of cyt *c* point towards subtle movements in general but more pronounced redox-induced changes at the heme propionate-7 as well as near the heme's covalent anchors.[34] Fig. 1 and Fig. S1 show the superimposed X-ray

structures of cyt *c* in both redox states. Compared to the X-ray structures,[27, 32, 33] the NMR solution structures[29-31] suggest somewhat more significant changes upon electron transfer. Redox-induced FTIR difference spectroscopy of cyt *c*, however, shows many distinct redox-dependent changes in the polypeptide backbone signature.[23, 24, 35, 36] These changes accounting for about 1% of the absolute amide I intensity seem to disagree with the minor ~~changes~~ movements observed in the X-ray crystal structures,[33] unless significant spectral differences are induced by charge redistribution. Nevertheless, attempts to assign FTIR bands to structural changes of redox-sensitive polypeptide segments of cyt *c* have been undertaken, based on the assumption that changes in some side chain orientations of some residues as well as alteration of their hydrogen

bonding patterns upon electron transfer would lead to local backbone rearrangements, hence leading to frequency shifts in the amide I modes.[23, 24, 35] However, recent crystal structures of horse heart cyt *c* obtained under similar crystallization conditions did not reveal such backbone rearrangements.[33]

In the following, we first describe out attempts to interpret the electrochemically-induced FTIR and femtosecond 2D-IR spectroscopy data in light of the literature assignments. Crucially, it is found that the additional dimension in 2D-IR spectroscopy highlights inconsistencies in

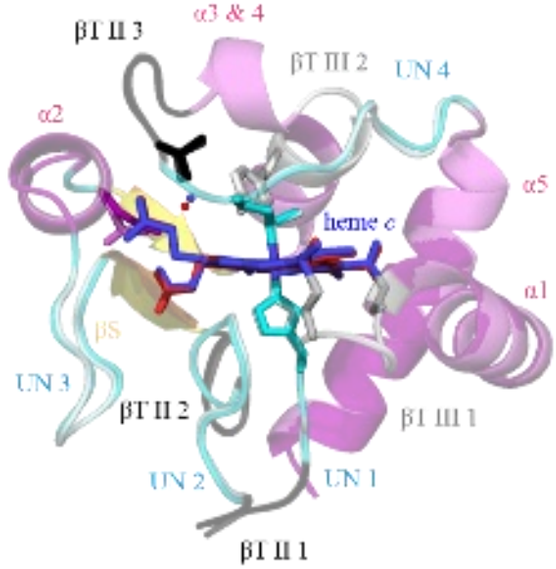

Fig. 1 Superimposed structures of horse heart cyt *c* in the Ox (dark colours, heme *c* in blue) and Red (light colours, heme *c* in red) (PDB 3O1Y and 3O20 for the Ox and Red states, respectively).[33] The secondary structure elements have coloured labels that correspond to same-coloured structural units and to the colour coding in Figs. 8 and S5. The heme *c*, the covalently bound Cys residues, the axial ligands as well as key residues (Asn52 in black, Tyr67 in magenta and Thr78 in orange) involved in redox-sensitive hydrogen bonding network are depicted as sticks. The water molecules Wat116 (Wat123 in the Red state) are shown as spheres.

the current assignments. In order to better understand how the complex difference spectra arise, we performed MD simulations and theoretical spectroscopy[37-40] which allowed us to assess the impact of changes in structure and charge state on the amide I contributions of the different secondary structure elements.

II. Results and discussion

Experimental results

FTIR difference spectrum. The difference spectroscopy approach is powerful for those samples which reveal only small spectral changes when the system is perturbed (Fig. 2, top row), in this case by a redox reaction. At first sight, the superimposed crystal structures of cyt *c* in both redox states shown in Fig. S1 present only very modest structural differences. Markedly different, the corresponding infrared difference spectrum shows distinct features that contain information about the changes occurring at the molecular level upon electron transfer. The Ox-minus-Red FTIR difference spectrum in the amide I' range of cyt *c* shows negative and positive bands arising from the Red and Ox states respectively as shown in Fig. 1C. Our data are consistent with previously published results[23, 24] for which assignments have been published.[24-26, 41]. The work by Ataka and Heberle, who used Surface-Enhanced Infrared Difference Absorption

Spectroscopy (SEIDAS) with different protein surface orientations induced by different surface functionalizations, is the starting point of the assignments presented here.[24] Table 1 and Fig. 2 provide an overview of current assignments according to literature.

Band	FTIR	2D-IR	Ref.	Assignment
$\mathbf{1}_{Red}$	1685	1683	1692-3[a, 24]	βT III
$\mathbf{1}_{Ox}$	1677	1676	1672[a, 24]	βT III
$\mathbf{2}_{Red}$	1665	1667	1661[a] -1666[b, 24-26]	βT III 1/ UN1/α1
$\mathbf{2}_{Ox}$	1656	1656	1653[b]-1658[a, 41]	UN/α
$\mathbf{3}_{Red}$	1653	1652	This work	UN1/α1
$\mathbf{3}_{Ox}$	1646	1644	1650[a, 25, 41]	UN/α
$\mathbf{4}_{Ox}$	1637	1632	1635[a, 24]	βS
$\mathbf{5}_{Ox}$	1629	??	N.A.	N.A.
$\mathbf{4}_{Red}$	1620	1623	1627[a, 24]	βS
$\mathbf{6}_{Ox}$	1612	1612	1612[a, 35]	βS
$\mathbf{7}_{Ox}$	1600	1606	1602[a, 24]	Heme *c* υ_{37} (Cβ=Cβ)
$\mathbf{5}_{Red}$	1588	1596	1595[a, 24]	Heme *c* υ_{37} (Cβ=Cβ)

Table 1 Overview of the observed signals' wavenumbers in the FTIR and 2D-IR difference spectra compared to values found in literature. The signals numbers correspond to the signal positions in the FTIR difference spectrum (shown in Fig. 2) for both the Ox and the Red states. The 2D-IR wavenumbers listed correspond to the observed GSB/SE features. The superscripts a and b refer to data recorded in H_2O and D_2O, respectively. The assignments are made according to the cited literature and the different protein regions are the same as in Fig. 1.

Principle of redox-induced 2D-IR difference spectroscopy of proteins.

Advantages of 2D-IR spectroscopy. The 2D-IR spectra are obtained by spectrally tuning a narrow pump beam with respect to a spectrally broad

probe beam. Similar to the FTIR absorption spectra of the two redox states of cyt *c* (Fig. 1A and B), the corresponding 2D-IR spectra show no clearly distinguishable redox-induced differences (Fig. 1D and E), necessitating the calculation of the redox-induced Ox-minus-Red 2D-IR difference spectrum (Fig. 1F). This spectrum features positive and negative signals on and off the diagonal.

As mentioned above, the FTIR spectra of the two-redox states are very similar, therefore the constructed difference incorporates significant cancelation effects. Overcoming such cancelation can be a major asset of 2D-IR difference spectroscopy, because the additional dimension can help to disentangle overlapping contributions (based on different vibrational couplings between oscillators; see below). Fig. 3 schematically illustrates cancellation effects in FTIR and 2D-IR difference spectroscopy.

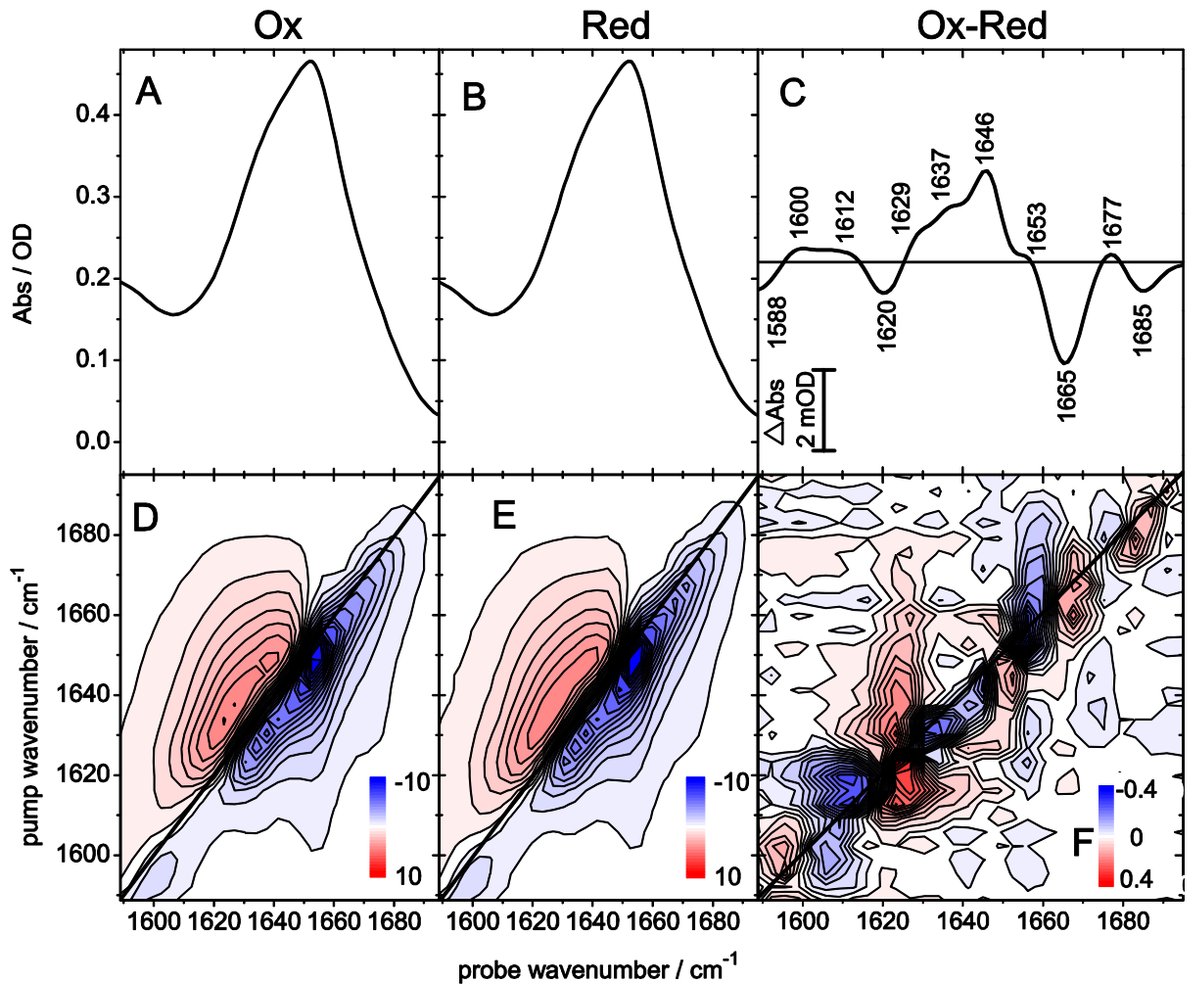

Fig. 2 Linear FTIR (A-C) and 2D-IR (D-F) spectra of the Ox (A, D) and Red (B, E) state as well as the Ox-minus-Red difference spectra (C, F). The 2D-IR difference data are recorded at 1.5 ps time delay. The diagonal is represented as a black line. The signal size is presented in mOD and each contour line corresponds to 0.677 mOD for the 2D-IR spectra of the Ox or Red states and 0.026 mOD for the 2D-IR difference spectrum.

Challenges in interpretation of amide I 2D-IR difference spectra. The Ox-minus-Red FTIR difference spectrum exhibits positive and negative bands arising from the Ox and Red states, respectively (Fig. 3A and B). In a 2D-IR spectrum the ground state bleach/stimulated emission (GSB/SE) and Excited state absorption (ESA) contributions are plotted conventionally as

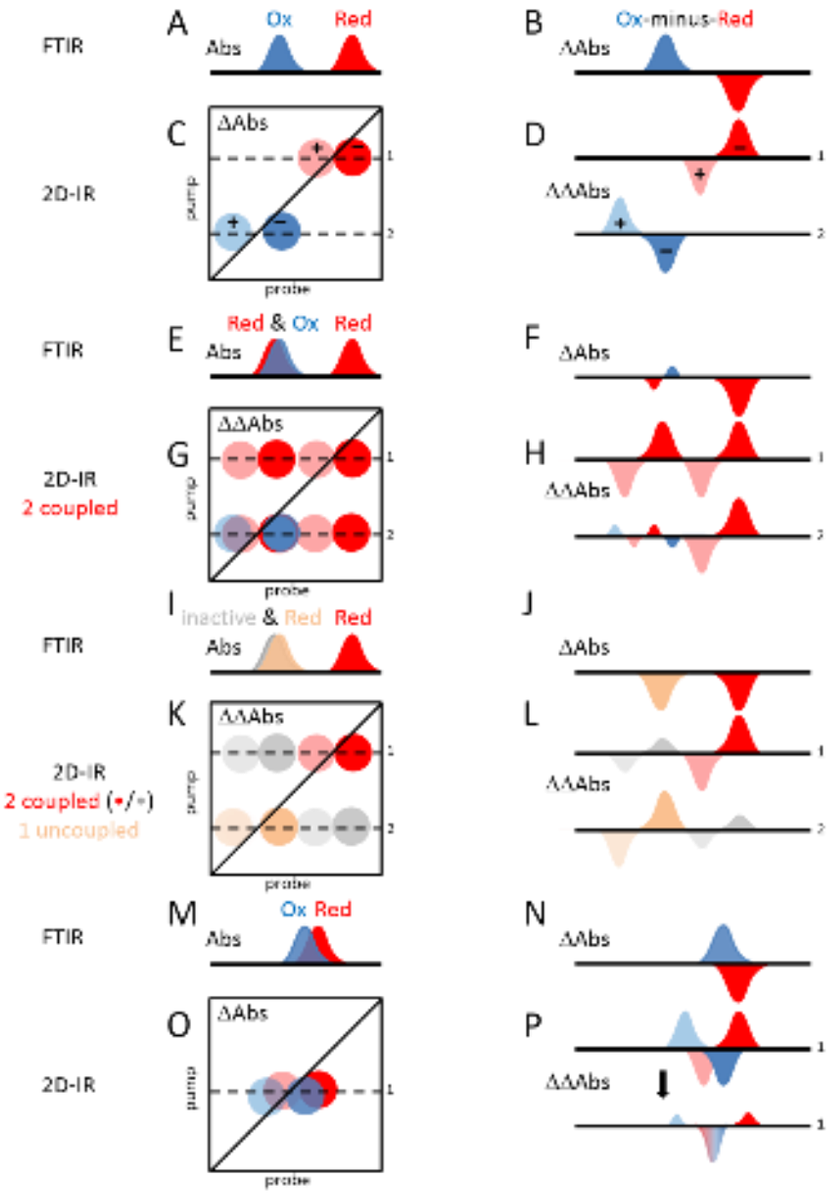

Fig. 3 Illustration of signals resulting from FTIR and redox-induced difference spectra for one oscillator which shifts upon oxidation (A and B). Panels C and D show 2D-IR spectra as well as spectral cuts along the probe axis for two different pump wavenumbers (dashed lines) of non-overlapping and uncoupled oscillators. The "+" and "−" signs refer to the conventional signs used in 2D spectroscopy, namely "+" for excited state absorption (light color) and "−" for ground state bleach/stimulated emission (dark color). Blue and red refer to the oxidized and red states respectively. Panels E and F show FTIR and redox-induced spectra of overlapping oscillators. Panels G and H depict the 2D-IR double-difference spectrum and cuts of coupled and spectrally overlapping oscillators. Panels I-L illustrate how mixtures of states (in this case between redox-active/inactive coupled states, and one uncoupled state) may result in a false 'conventional' cross-peak pattern, evident by incorrect cross-peak intensities (panel L). Panels M-P show the effect of adding GSB/SE of one redox state and ESA of the other redox state in the difference spectrum. The diagonal in the 2D-IR spectra is represented by a continuous line.

negative and positive signals,[13] respectively, and the Ox-minus-Red operation flips the conventional signs of the Red state's signal (Fig. 3C and D). The Ox-minus-Red subtraction is a clear advantage for FTIR difference spectroscopy, as well as for systems exhibiting only few and spectrally distant features (like shown in Fig. 3 C). Whenever FTIR absorption bands arising from Ox and Red overlap (Fig. 3E), as is the case for cyt *c*, they cancel out to some extent in the redox-induced FTIR difference spectrum (Fig. 3F). Similarly, the diagonal peaks of overlapping bands of Ox and Red will cancel in a 2D-IR difference spectrum (Fig. 3H, cut 2). However, if one of the Red bands is coupled to another band, cross-peaks are generated (Fig. 3G). Such couplings are likely to occur for a system with many oscillators like cyt *c*. While the diagonal peaks of Red and Ox cancel in cut 2, the cross-peak belonging to the band of the Red state can be clearly observed. In this fashion, bands that are obscured by (partial) cancelation in an FTIR difference spectrum might be detected through couplings in a 2D-IR difference spectrum.

It is however also possible that redox-active bands shift in wavenumber and intensity differences remain invisible. Consider the case of three oscillators, two being redox-active and one inactive (Fig. 3I). The inactive one cannot be seen in the difference spectrum (Fig. 3J) and also not in the

2D difference spectra (Fig. 3K-L). The inactive one and one of the active oscillators are weakly coupled. The other oscillator is not coupled. While the inactive one is not affected by redox switching and therefore does not appear in the 2D difference spectrum, it still generates a cross peak with the redox-active oscillator. The third uncoupled one will off course still contribute to the 2D-IR spectrum. However, if it has the same vibrational frequency as one of the first two coupled oscillators belonging to the other redox state, then the cross-peak of the first pair of oscillators will appear on the off-diagonal, while one diagonal signal will cancel out by the third oscillator (Fig. 3I), falsely restoring the characteristic square pattern in the 2D-IR difference spectrum. This is a situation that is likely also encountered in our cyt *c* data, see below. A detailed analysis of the extinction coefficients would however in principle allow for the distinction between a conventional square cross-peak pattern and a pattern resulting from a mix of the mentioned three oscillators. Another issue arises in cases where it is difficult or impossible to excite a single oscillator in an absorption band where many modes overlap. The presented measurements in the amide I region are a good example in that respect, where strongly overlapping contributions exist of several secondary structure elements such as α-helices, β-sheets, and unordered structures. The infrared band of

predominantly β-sheets structures shows for instance many coupled vibrational modes[14] which have been shown to be redox sensitive[42].

Because we are interested in redox-induced changes in 2D-IR spectra, we subtract the 2D-IR spectra from each other. Conversely, the GSB/SE of the Red state might overlap with the ESA of the Ox state, causing the two contributions not to cancel but to add up (illustrated in Fig. 3M-P, and possibly occurring in the cyt *c* data as well, see below). Hence the Red and Ox states would together give rise to a "negative" signal near the diagonal. Band positions in the Ox-minus-Red 2D-IR spectrum show a slight shift compared to the FTIR difference spectrum because of overlapping contributions of ESA and GSB/SE of the same mode. Fig. S2 in the **Supplementary material** shows a comparison between the FTIR difference spectrum and the projection of the 2D-IR difference spectrum in Fig. 1C on the probe axis. Note that one redox state cannot exhibit a cross-peak with the other redox state. The applied potentials yield the full Ox- or full Red-state from which the difference spectra are calculated. Thus, intermolecular Ox-to-Red couplings can be excluded.

Due to the complexity of the redox-induced 2D-IR difference spectrum of cyt *c*, we use cuts (Fig. 4) through the 2D-IR difference spectrum at selected pump wavenumbers to discuss the assignments especially when strong

overlap between signals from the Ox and the Red states occurs. The measured cuts are interpreted in a way that is analogous to what was done for the examples show in Fig. 3 above. We encounter however several difficulties assigning the spectral features, prompting us to perform MD simulations which expose fundamental underlying problems associated with the conventional way of interpreting amide I difference 1D-IR and 2D-IR spectra in this fashion.

Discussion of selected cuts along the literature assignment.

The 2D-IR difference spectrum of cyt *c* after 1.5 ps is shown in Fig. 1F. The cuts through the 2D-IR spectrum are compared to the features in the FTIR difference spectrum in Fig. 1C, where 7 signals are assigned to the Ox state and 5 to the Red state according to literature (see Table 1). The colour of the labels in Fig. 4 indicates the species that is held responsible for the signals, i.e. blue for Ox and red for Red. Noise level and scattering contributions to the 2D-IR difference spectrum at negative times and at 1.5 ps are shown in Fig. S3 and S4, respectively (**Supplementary material**). In order to make the connection between the FTIR and 2D-IR data easier, the FTIR difference spectrum shown in Fig. 1 is repeated in Panel A of Fig.

4 where panels B and C each show two cuts at neighbouring pump frequencies. For the analysis of the 2D-IR difference data in Fig. 4 the following simple assumptions where made: 1) If a GSB/SE is observed at a certain pump frequency a corresponding ESA contribution (symbolized by a *) should appear at lower wavenumbers due to the anharmonicity (see Fig. 3C-D). 2) Although we have pure Ox and Red species, the 2D difference spectra of course contain cancelling or additive contributions of both (see Fig. 3G-H and Fig. 3O-P). However, a cut through the 2D-IR spectrum can feature signals that might be either attributed to a single species or to a mixture of the two due to spectral overlap. 3) The pumped species usually can be determined by matching the absorption (i.e. via the FTIR difference spectrum) to the sign of each feature (see Fig. 3C-D). 4) Coupled signals belong of course to the same redox state and should have matching absorption features (see Fig. 3G-H). It is worth emphasizing that signals obtained from a 2D-IR experiment scale with the square of the extinction coefficient, ε^2, while the FTIR signal scales only with ε; hence, if a signal of the Ox state and an equally-sized signal of the Red state are caused by different numbers of oscillators, they may cancel out in the FTIR difference spectrum, but their according signals in the 2D-IR spectrum do not cancel.[20] Using the assumptions described above, the cuts in Fig. 4 are

discussed. The green pump pulse, depicted by the Lorentzian pulse below the pairs of curves in Panel B, yields a bleach from the signal $\mathbf{1}_{\mathbf{Red}}$ which has a cross-peak with the signal $\mathbf{2}_{\mathbf{Red}}$ (the upgoing feature). If the $\mathbf{2}_{\mathbf{Red}}$ feature is pumped (the orange pulse), cross-peaks appear with signals $\mathbf{1}_{\mathbf{Red}}$ and $\mathbf{4}_{\mathbf{Red}}$. Note that the peak locations of the features are slightly different in Fig. 4B and C which could be due to different cancellation effects depending on the pump wavenumber. It should be noted that the pump pulse excites all the secondary structure elements absorbing at the pumped wavenumber, and the signal $\mathbf{1}_{\mathbf{Red}}$ in the 2D-IR is what is left after the cancellation between the Ox and Red spectra of the protein. According to previous assignments[24, 35, 36], band $\mathbf{1}_{\mathbf{Red}}$ arises from β-turns type III (βT III

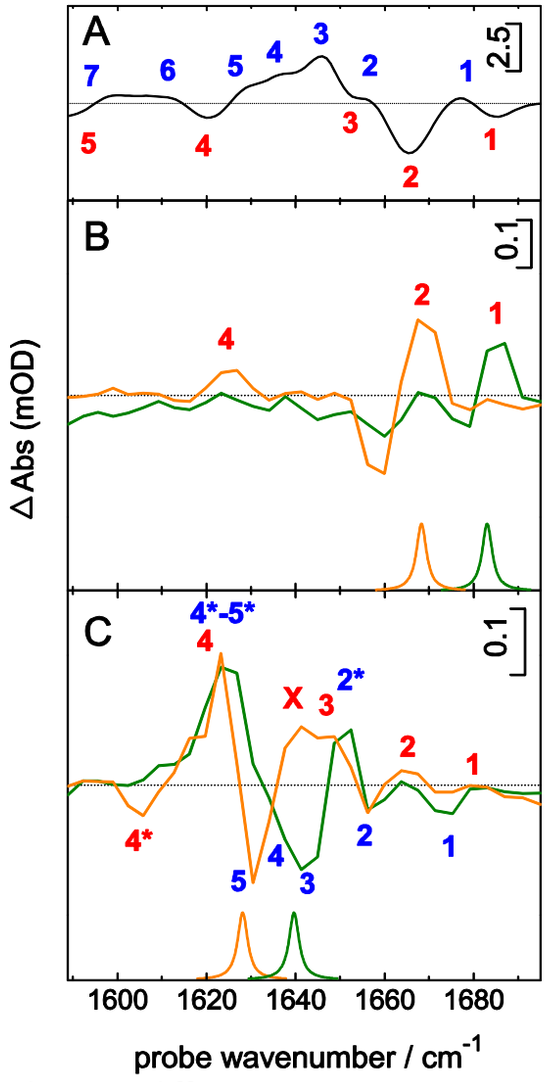

Fig. 4 Panel A depicts the FTIR difference spectrum as a reference for the signal's positions in the 2D-IR difference spectra with the difference signals numbered from $\mathbf{1}_{Ox}$ to $\mathbf{7}_{Ox}$ for the Ox state in blue and from $\mathbf{1}_{Red}$ to $\mathbf{5}_{Red}$ for the Red state in red. Panels B and C show selected horizontal cuts of the 2D-IR difference spectrum shown in Fig. 1. The pump position for each cut is visualized by a narrow-band Lorentzian pulse shown at the bottom of each panel (with its colour corresponding to the resulting collected spectrum). The numbers with asterisks highlight some of the observed ESA and $\mathbf{X}_{Red}$ indicates a 2D-IR difference signal of the Red state with no corresponding FTIR difference signal. The same numbers are used in panels C-H that show two cuts each, corresponding to neighbouring high (green lines) and low (orange lines) pump wavenumber. The subscripts $_{Ox}$ and $_{Red}$ are omitted from the signal numbers for clarity. The black horizontal dotted lines represent y=0. The vertical bars represent the vertical scale unit in mOD.

assignment of the signal $\mathbf{2}_{\mathbf{Red}}$ is more controversial since it was previously assigned to β-turns type II,[24] β-turns type III or an α-helix.[23, 35] A fourth assignment is the one made by Marboutin *et al*.[26] where it was assigned to residues 14-21 (Horse heart cyt *c* numbering) that form the backbone of microperoixdase-8 (this part of the structure is labelled βT III 1 as well as unordered structure UN1 in Fig. 1). The structure of cyt *c* actually contains two β-turns type III formed by two sets of residues, namely the residues 14-19 and 67-70 (βT III 1 and βT III 2 in Fig. 1, respectively).[27] These two protein segments lie on opposite sides of the heme and are separated by 49 residues, so that vibrational coupling between them is unlikely due to spatial separation. Both signals $\mathbf{1}_{\mathbf{Red}}$ and $\mathbf{2}_{\mathbf{Red}}$ could therefore be assigned to the backbone vibration of residues 14-19. Although the redox-induced 2D-IR difference spectrum shows mainly redox-active contribution on the diagonal, the data might yet show coupling between a redox inactive βT III (i.e. it is not visible in the electrochemically-induced FTIR difference spectrum) and a redox active one (as depicted schematically in Fig. 3I-L). Therefore, the observed cross-peak can be possibly arising from a single βT III, for instance βT III 1 which is known to be redox-sensitive, or βT III 2 which was not reported to be redox-active. The two βT III segments, however, are too far away to be directly coupled.

As we are measuring at a population time of 1.5 ps, also vibrational energy transfer (VET) might occur. However, on this time scale VET is unlikely to create cross-peaks between distant segments as typical timescales for VET through bonds (and not between segments) are 4 Å ps^{-1} and through non-covalent contacts even slower.

The signal $\mathbf{2}_{\mathbf{Red}}$ also shows a cross-peak to the signal $\mathbf{4}_{\mathbf{Red}}$ which had been previously assigned to β-sheets[24] (the dark yellow label βS in Fig. 1). The amide I' modes of β-sheets are known to be split into two low and high-frequency modes with the low frequency one having the highest absorption coefficient.[19, 43, 44] Accordingly, signal $\mathbf{4}_{\mathbf{Red}}$ must have a counter-part in the high-frequency end of the amide I' which should appear near or at the signal $\mathbf{1}_{\mathbf{Red}}$ in the FTIR difference spectrum, which was assigned to βT III (see above). Therefore, a contribution from β-sheets to the $\mathbf{1}_{\mathbf{Red}}$ signal cannot be excluded at this stage.[45, 46] However, if that was the case, then the cross-peak should be more pronounced between signal $\mathbf{4}_{\mathbf{Red}}$ and signal $\mathbf{1}_{\mathbf{Red}}$ than between $\mathbf{2}_{\mathbf{Red}}$ and $\mathbf{4}_{\mathbf{Red}}$, which is not the case here. Therefore, $\mathbf{1}_{\mathbf{Red}}$ could be assigned to βT III 1. Possibly, the high-frequency mode of β-sheets either has a small absorption coefficient, or signal $\mathbf{4}_{\mathbf{Red}}$ is not arising from β-sheets in the first place. Nevertheless, the assignment of signal $\mathbf{4}_{\mathbf{Red}}$ to other secondary structure components is not reasonable based on the

literature since no other secondary structure element is expected to absorb at this low frequency.[46] According to the FTIR literature assignments, Panel B shows predominantly coupling between signal $\mathbf{1}_{\mathbf{Red}}$ (βT III 1) and $\mathbf{2}_{\mathbf{Red}}$ (βT III 1, UN1 and α1) and between $\mathbf{2}_{\mathbf{Red}}$ and $\mathbf{4}_{\mathbf{Red}}$ (βS). The contribution of βT III 2 to the coupling to βS is not likely. The β-sheets in cyt *c* are close to the propionate edge of the heme *c* whereas the redox-dependent signature of βT III had been assigned to the one bearing the covalently-bound Cys. These sheets undergo a very slight structural readjustment of their backbone upon electron transfer (see the X-ray structures in Fig. S1 in the **Supplementary material**) and it is unclear if this is sufficient to shift the β-sheet's absorption frequency, leading to the difference signature of signal $\mathbf{4}_{\mathbf{Red}}$ observed in the difference spectrum. An alternative explanation would be that the change in charge distribution is the main reason for the shift. Importantly, however, the coupling observed between the band $\mathbf{4}_{\mathbf{Red}}$ (attributed to β-sheets) and band $\mathbf{1}_{\mathbf{Red}}$ and $\mathbf{2}_{\mathbf{Red}}$ (attributed to βT III) cannot be explained in light of the distance that separates the two structure elements (see Fig. 1). Alternatively, the cross-peak might arise from energy transfer during the waiting time of 1.5 ps. However, it has been reported that the transfer rate between two residues connected by a covalent bond[47] is $(0.5\ ps)^{-1}$ and non-covalent transport is

at least one order of magnitude slower,[48] we therefore rule out energy transfer over such long distances as a source of cross-peaks.

The spectral cuts shown in panel C of Fig. 4 contain features that are attributed to a mixture of different redox states. Exciting with a pump pulse at the low pump wavenumber (the orange pulse and its corresponding orange cut through the 2D spectrum) shows cross-peaks that are also observed in the green cut (signals $\mathbf{1_{Ox}}$ and $\mathbf{2_{Ox}}$). However, major differences occur at lower frequencies. Firstly, the orange spectrum shows a negative feature directly at the pump wavenumber which corresponds to the $\mathbf{5_{Ox}}$ feature of the FTIR difference spectrum. The orange pump pulse also overlaps with $\mathbf{4_{Red}}$, resulting in the negative $\mathbf{4^*_{Red}}$ feature at 1605 cm^{-1}. The green spectrum, resonantly excited at the position of $\mathbf{3}$-$\mathbf{4_{Ox}}$ shows also a clear positive signal at the location of $\mathbf{4^*_{Red}}$, but now they arise from $\mathbf{4^*_{Ox}}$ and $\mathbf{5^*_{Ox}}$. The orange spectrum shows a broad positive feature around 1640-1650 cm^{-1}, which cannot be $\mathbf{4^*_{Ox}}$ (that would appear around 1630 cm^{-1}). This feature must originate from the Red species underlying the set of signals $\mathbf{3_{Ox}}$-$\mathbf{5_{Ox}}$, because excitation of these modes would result in a negative feature here, thus the orange spectrum is a mixture of Ox and Red states (see also below). In essence, the cross-peaks observed in the green spectrum of Panel C point towards the coupling

between the excited signals $\mathbf{3_{Ox}}$-$\mathbf{4_{Ox}}$ and $\mathbf{1_{Ox}}$ and $\mathbf{2_{Ox}}$. According to the literature, this would correspond to a coupling cross-peak between UN1/α1, βS, and βT III 1, which is again unlikely due to their large spatial separation.

Panel C shows that $\mathbf{4^*_{Ox}}$-$\mathbf{5^*_{Ox}}$ overlaps with the GSB/SE of $\mathbf{4_{Red}}$ (as illustrated in Fig. 3M-P). Yet, the excitation of signal $\mathbf{4_{Red}}$ (1623 cm^{-1}; orange curve) gives rise to cross-peaks of positive signs at 1649 cm^{-1} (signal $\mathbf{3_{Red}}$) and 1641 cm^{-1} (signal $\mathbf{X_{Red}}$). This $\mathbf{X_{Red}}$ does not have an equivalent in the FTIR difference spectrum, therefore we call it '$\mathbf{X_{Red}}$'. Interestingly, $\mathbf{X_{Red}}$ appears in a spectral range that is dominated by (positive) absorption signals from the Ox state in the FTIR difference spectrum (see Fig. 4A). The $\mathbf{X^*_{Red}}$ signal in the FTIR is expected to appear at similar wavenumbers as $\mathbf{5_{Ox}}$, hence an overlap of the two is very likely. Bands $\mathbf{3_{Red}}$, $\mathbf{4_{Red}}$ have been assigned to α-helix, unordered structures and β-sheets which correspond to UN1/α1, and βS, respectively. Band $\mathbf{X_{Red}}$ is tentatively assigned to one or more of the same structural units because these signals appear here for the Ox state as well (bands $\mathbf{3_{Ox}}$-$\mathbf{5_{Ox}}$). Note that there are more Ox than Red signals in the measured spectral range, which, however, is not a valid argument for the novel $\mathbf{X_{Red}}$ signal. If $\mathbf{5_{Ox}}$ (βS in Fig. 1) contributes to the orange spectrum, then it is coupled to $\mathbf{1_{Ox}}$ and $\mathbf{2_{Ox}}$ which in turn are coupled

to signals $\mathbf{3_{Ox}}$ and $\mathbf{4_{Ox}}$ (UN1 and βS in Fig. 1, respectively). To summarize, the coupling patterns observed here (i.e. between βS and βT III 1 in one case and between UN1/α1 and βS in another case) do not match with the literature assignment because of the long distances that separate the involved segments and making any observation of coupling impossible. In summary, the discussed cuts appear to suggest couplings that are difficult to explain based on previous literature assignments. In fact, cross-peaks pointing towards the unlikely coupling between two far-apart segments of cyt *c* raise suspicions about the literature assignment and interpretation of the FTIR difference spectrum of cyt *c*, and prompt us to perform computational spectroscopy based on MD simulations to understand the disagreement between the literature assignments and the observed couplings in the 2D-IR difference data.

Theory results

A detailed analysis of protein 2D-IR spectra in general and of cyt *c* in particular is challenging due to several factors such as the complexity of the protein itself, spectrally overlapping signals, the coupling of backbone modes, vibrational energy transfer, as well as the relatively short lifetime of the vibrationally-excited state. Accordingly, combining MD simulations

with quantum mechanical response function calculations is thought to be a sound approach to help explain the experimental FTIR and 2D-IR data.

FTIR difference spectrum. For each redox state the performed MD simulations yielded two individual trajectories, which were clustered into time ranges containing similar structures (see the Theory section in **Supplementary material**). The FTIR and 2D-IR spectra were then calculated for each of the 46 sub-trajectories. These were identified in a 35 ns molecular dynamics trajectory based on differences in Ramachandran angles using both the oxidized and the reduced Hamiltonians. Realizing that the true structures are unlikely to be sampled correctly with a single MD simulation, the spectra of the 46 sub-trajectories were used as a basis for fitting the FTIR difference spectrum. A least-square fit procedure was employed to fit the spectrum. The error minimized in this procedure included the sum of the root-mean-square-deviation between the simulated and experimental difference and full FTIR spectra. The root-mean-square-deviation for the difference spectrum was weighted with a factor of one thousand to compensate the smaller intensities of the difference spectrum as compared to the full spectra. The inclusion of the plain FTIR spectra ensures that the relative intensity of the difference spectrum is well reproduced. The final fit of the difference spectrum is

shown in Fig. 5A and the fitting coefficients of the sub-trajectories are shown in Fig. 5B. Overall, the difference spectrum is reproduced quite well and only a handful of sub-trajectories significantly contributes to the Red form, while in the order of ten sub-trajectories significantly contribute to the Ox form.

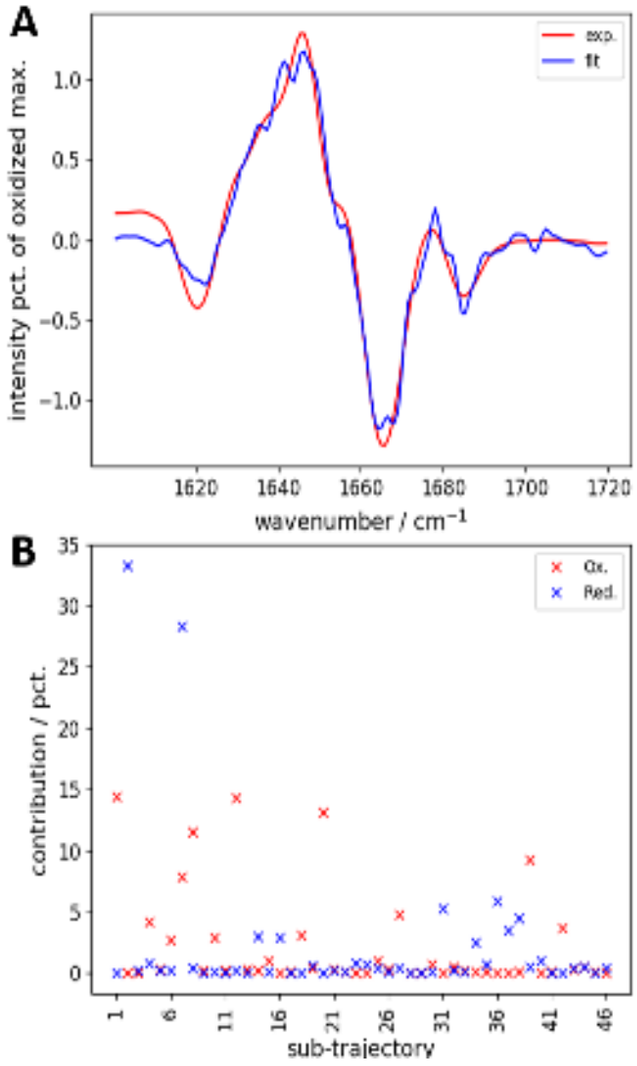

Fig. 5 A. Comparison of the fitted and simulated FTIR difference spectra (oxidized-reduced cytochrome *c*). The intensity is given in the relative strength compared to the maximum of the amide I band of the oxidized species. B. The contribution of the 46 difference sub-trajectories to the fitted FTIR difference spectrum of cytochrome *c*.

The contributions to the difference spectra were further analysed. We calculated the absolute spectra using the Hamiltonians of the differently charged states, but now using the structures according to the *average* of the weights taken from the Red and Ox sub-trajectory. This represents the spectrum one would obtain if the change in redox state only was the charge on the heme group and the structure was a fixed average of the Ox and Red structures. The spectral changes observed in this fashion are, thus, solely determined by frequency shifts caused by the change of charge. The average difference spectrum based on solely the charge contribution is plotted in Fig. 6 (red spectrum). Similarly, absolute spectra were calculated using the average Hamiltonian of the Ox and Red charge states, but now using the different sub-trajectory weights. This spectrum represents the spectrum that one would obtain if the change in redox state was only cause by structural changes (blue spectrum). The full difference spectrum is theoretically given by the sum of the charge and structure contribution

spectra as defined above and resembles the experimental (black) spectrum, as shown in Fig. 6. In general, however, the charge contribution spectrum resembles the full spectrum the most and the structure contribution spectrum actually has the opposite sign over a broad range of frequencies. This means that the direct effect of the change in charge itself is at least as important for the infrared difference spectrum as the structural change induced by changing the charge. When changing the redox state, the frequency changes due to the change of the local electric field can thus not be neglected. Furthermore, the structure change leads to the opposite sign of the signal in most frequency regions. This is very important for the interpretation of the overall spectra. For the peak at 1620 cm^{-1} and the peak at 1685 cm^{-1} the overall sign is, however, the same

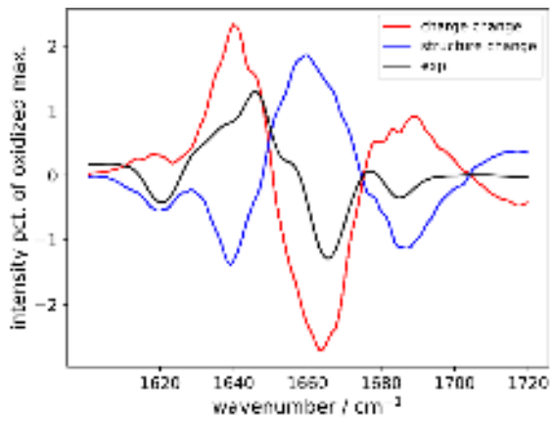

Fig. 6 The difference spectra obtained from theory, separated into contributions from the charge change and the structure change, are compared to the experimental difference spectrum. The sum of the two is the computed difference spectrum shown in Fig. 5A. The intensity scale is normalized to the maximum of the amide I absorption band of the Ox species.

as that resulting from changing the structure. Typically, FTIR difference spectra are assigned solely based on structural changes. The present results demonstrate that this is insufficient, at least when the charges in the two protein structures are different e.g. due to a change of protonation, ion binding or redox state, as that induces a large change in the local electric fields and creates a substantial contribution to the difference spectrum. Furthermore, the structure change contribution may have the opposite sign of that resulting from the charge change and the result of the structure change may thus be the opposite of what one would conclude if only the structural effect is considered. We further examined this effect by calculating the change in the average local site frequencies and the effect of charge and structure changes on these. The result is shown in Fig. S6 and Fig. 7, where it is clear that the changes are very large (>10 cm^{-1}) on a few sites, while at most other places the changes are modest but clearly non-zero. The charge difference leads to larger changes and the key sites are residue 28, 29, as well as units around residue 80 (see Fig. S6). These sites are all in the vicinity of the heme group (see Fig. S5 panel A in the **Supplementary material**). The effect of changing the redox state on the couplings is more challenging to analyse. We defined a simpler quantity, which we denote the coupling-strength.[49] This is defined as the

sum of all signed couplings of one selected site to all other amide I sites. This result in one coupling-strength for each amide I site, significantly simplifying the analysis. For simple linear structures this coupling-strength determine the shift of the collective absorption peak.[49] An obvious drawback is that anti-correlated changes in couplings to the same site may be hidden in the analysis.

Overall we observe that the coupling-strength changes little compared to the site frequencies (Fig. 7, see Fig. S6 for a version that distinguishes

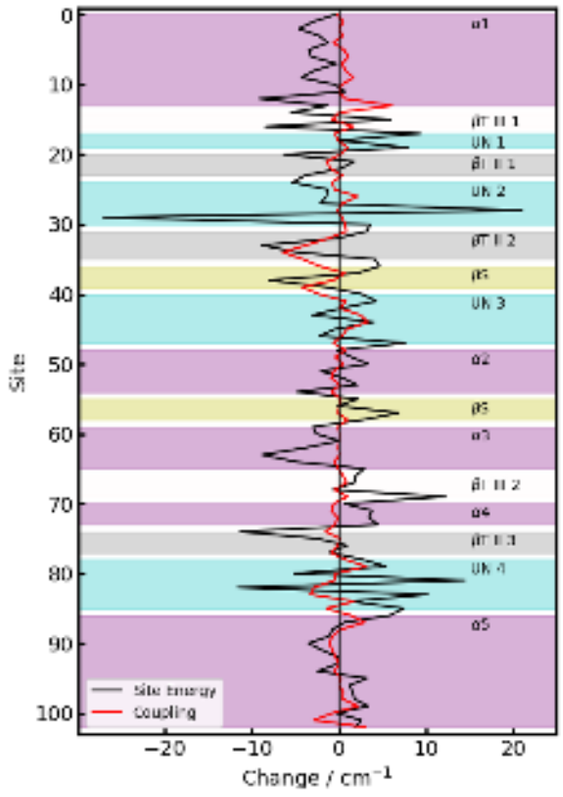

Fig. 7 The change in the average site frequency compared to the change in the coupling strength. The different structural elements (see Table 1) are highlighted by background colouring (corresponding to the colours in Fig. 1).

between charge and structure distributions). The largest coupling change is 6.5 cm^{-1} while the largest site frequency change is 27 cm^{-1}. In the way the couplings are obtained here, they only depend on structural changes and are independent of the change in the local electric field. This analysis shows that the changes in regions near the heme group are the largest, while small changes are found throughout the protein.

Typically, FTIR difference spectra are interpreted by assigning signals in the spectrum to certain parts of the protein's secondary structure (see Table 1 and the literature cited therein). In the discussion of the 2D-IR spectra in the experimental section above we attempted to follow this approach as well and encountered obvious inconsistencies. We therefore proceeded to calculate the FTIR difference spectra for the individual different structural segments (e.g. for each α/βT II/etc. unit separately) which have been used in the literature assignments and which are defined by the residue numbers in Table S2 in the **Supplementary material**. This was achieved by insertion of a segment projection operator in the response function[50] governing the FTIR signal (Eq. 2 in **Supplementary material**), that is weighting the contribution of each eigenstate to the segment spectrum by the population of the eigenstate on that specific segment. The total sum of the segment spectra is equal to the overall

absorption spectrum. The resulting individual segment spectra for the Ox and Red states are shown in Fig. S7 and S8 of the **Supplementary material**, respectively. The resulting difference spectra of each of the segments are shown in Fig. 8 (the sum of all individual segments for each secondary structure type is shown in Fig. S9). Here is it clear that, to some degree, essentially *all* segments contribute to the spectral changes throughout the full amide I spectral region. It is noteworthy that the contribution of the large C-terminal α-helix (the magenta α5 spectrum) is negligible. It is also important to see that most segments contribute at a broad range of frequencies, questioning the interpretation of the spectra in terms of spectrally narrow contributions of a few segments as is usually done in the FTIR literature. Furthermore, except for a few residues (in particular 28-29, see Figure S6) both structure and charge changes contribute to the frequency changes. With the segment-specific spectral contributions in hand (see Fig. 8), it is obviously difficult to attribute specific features in the experimental difference spectrum to a particular structural unit because of spectral overlap and/or sign-compensating features. For instance, the experimental difference peak at 1620 cm^{-1} (at the first vertical dashed line) has a dominant contribution from the βT III 2 segment (residues 66-69). Still, tails from other segments are present and a contribution from α1

(residue 1-13) with opposite sign but similar magnitude compared to that of βT III 2 is present as well. The peak at 1635 cm^{-1} has contributions from α1, UN 2, and βT II 3, while opposite sign contributions predominantly arise from α4, UN 4, and βS. The peak at 1646 cm^{-1} has contributions from α3, with an opposite sign contribution from for instance UN 3. In the region between 1640 cm^{-1} and 1665 cm^{-1} many contributions and tails of contributions are present, making an assignment too complex. The peak at 1665 cm^{-1} has contributions from UN 1, UN 2, and α3 while α2, UN 4, βT II 1, βT II 2, and βS provide opposite sign contributions in this region. The peak at 1685 cm^{-1} has contributions from βT II 1, βT II 2, and βT II 3 and βS,

while α4, the UN segments, and βT III 3 have opposite sign contributions. Overall, the difference spectrum of the whole protein is actually *smaller* in signal size than the difference spectra of many of the individual segments.

To summarize, the interpretation of the FTIR difference data based on the MD simulations shows that *all* the different segments of cyt *c* contribute *throughout* the full amide I spectral region. Therefore, the

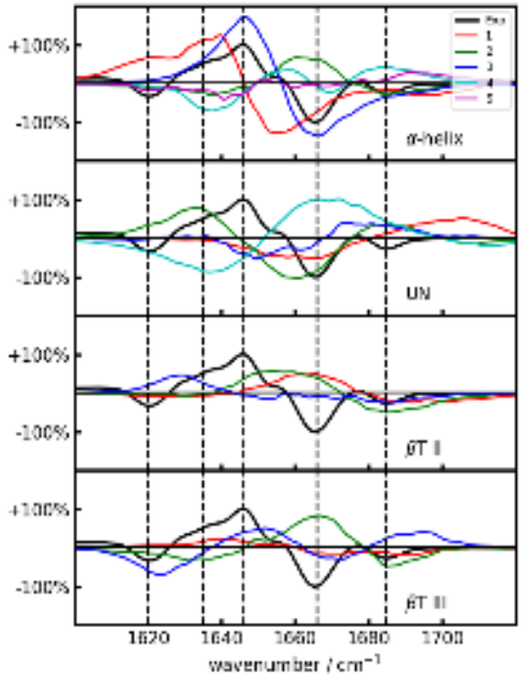

Fig. 8 The difference spectra for different secondary structure segments of cytochrome *c*, compared to the experimental difference spectrum (black). Segment numbers are according to Fig. 1 and Fig. 7. For instance, the red spectrum in the top panel corresponds to α-helix 1. The green βT III spectrum in the bottom panel is the βS element. For assignment details see Table 1). The vertical lines highlight the frequencies of the main maxima and minima of the experimental infrared difference absorption signals.

interpretation of the amide I difference signals as arising from changes in

distinct segments of structure as usually done in the FTIR literature is not valid in the present case. Estimating the secondary structure content from an amide I absorption spectrum or 2D-IR spectrum is possible,[38, 51-53] as well as measuring changes in secondary structure content in the context of large structure changes.[12 38, 54, 55] However, the present findings suggest that the assignment of a particular feature in a FTIR difference or 2D-IR difference spectrum to *a particular secondary structure element of the protein* is typically not feasible.

In a 2D-IR spectrum, cancelation effects are even more prevalent, as cross-peaks may arise from a singular segment or from two adjacent segments. Moreover, the construction of an Ox-minus-Red difference spectrum, with Red and Ox already being difference spectra (each having positive ESA and negative GSB features), may obscure the origin of each feature as well. One could thus conclude that the off-diagonal signals may result from cancelations of various cross-peaks having various signs and shapes which lead to far more off-diagonal spectral features than there actually are. To demonstrate this, the two-dimensional spectrum was calculated for the Ox and Red species using the same sub-trajectory weighting factors as obtained for the one-dimensional fit (see Fig. S10 in **Supplementary material**). The resulting difference spectra are shown for

0 and 1.5 ps time delays in Fig. 9. The two-dimensional difference spectrum has a large number of off-diagonal features making it very challenging if not impossible to interpret. This is not only because 2D-IR spectra of either species both have negative and positive features resulting from bleach and excited state absorption features, but also because different segments may also contribute with different signs. Furthermore, due to the dependence of the individual contributions to the 2D-IR spectra on the extinction coefficient squared,[56] highly delocalized/coupled states tend to contribute more in the spectra.[57] This delocalization further leads to smaller effective anharmonicities and an increased interference between absorptive and bleach features. Furthermore, the difference spectrum is varying a lot as a function of population time delay. While a direct comparison between predicted and experimental spectra is tempting, such a comparison is very challenging as the simulations do not take into account occurring thermalization effects[58, 59] and relaxation-assisted cross-peaks[60, 61] arising during the population time delay. Also, due to a finite pulse duration, the experimental data cannot be obtained without artifacts for zero time-delay. Furthermore, the 2D-IR spectra are very sensitive to the accuracy of the couplings in the simulation and even small deviations in the overall spectra may result in large ones when the

difference spectrum is taken. With future improvement of experimental and simulation procedures, a simultaneous fitting based on the FTIR as well as 2D-IR spectra may be within reach. However, it may be more fruitful to employ isotope labelling methods[17, 18, 62-69] or IR labels[70-78] to reveal information on local structural changes.

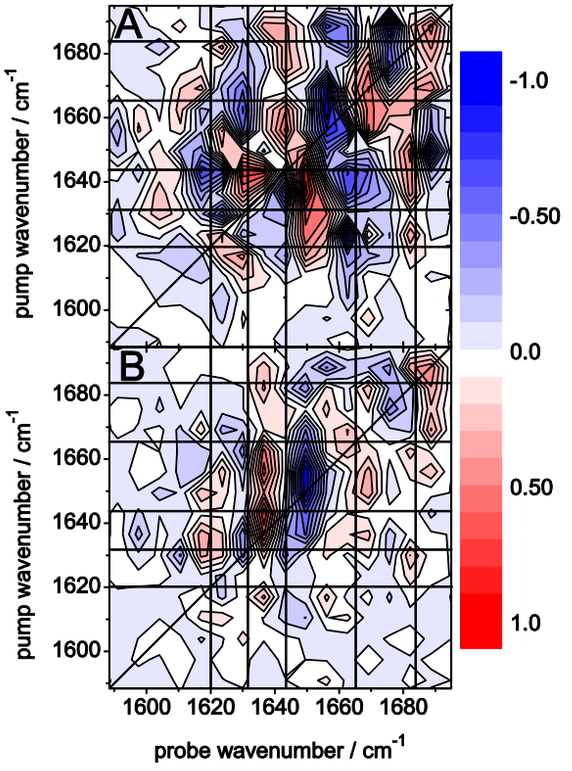

Fig. 9 The simulated 2D-IR Ox minus Red difference spectra for 0 ps (A) and 1.5 ps (B) time delays. Each contour line represents 5% of the total signal size. The black lines highlight the frequency of the maxima of the experimental infrared signals. The horizontal and vertical lines correspond to the peak positions observed in the FTIR difference spectrum.

A noticeable difference between the simulated and experimental 2D-IR difference spectra is the absence of the 1620 cm^{-1} peak in the simulated spectrum (Fig. 9). This peak is dominant in the experimental 2D-IR

difference spectrum. In the FTIR difference spectra in Fig. 5A this peak is present both in the experimental and fitted data. We tested the importance of this feature by repeating the fit of the FTIR spectrum in Fig. 5A, but this time excluding the spectral region up to 1630 cm^{-1}. The data are shown in the **Supplementary material** Fig. S11-S13. In the resulting fit only the peak at 1620 cm^{-1} disappears (compare Fig. 5A with Fig. S11). Both the weight of the different sub-trajectories as well as the contributions of the individual structural segments are not changing significantly (compare Fig. 5B with Fig. S12 and Fig. 8 with Fig. S13). We therefore, conclude that the 1620 cm^{-1} peak in the fitted spectra may arise due to overfitting. The overall conclusion of the paper is however not affected. Regardless the fitting procedure, the peaks dominating the difference FTIR spectrum arise from contributions from changes in charge environment and structural changes in multiple segments. As before, the contribution from any one given segment to the difference spectrum is affecting almost the full spectral range. We speculate that the origin of the experimentally observed 1620 cm^{-1} peak is due to a very limited number of optical transitions. While this could in principle be a thus far unknown vibration in the heme *c* group, it is more likely that it arises from a single structural segment. It should be noted that a heme vibration (i.e. the so-called C_a=C_b

vinyl stretching) had been found at about 1620 cm^{-1} in various other heme types, but not in type-*c* heme groups[79-81] like in cyt *c*, since this vinyl group is lost in the covalently-bound heme *c*. The present simulations are inherently biased toward the 1AKK starting structure, which presumably describes the oxidized structure better. It may be that we cannot describe a part of the occurring structural change in the reduced structure with the current simulation procedure and more extensive simulations (for example replica exchange[82] simulations) may be needed to catch this change. Such approach, however, will also pose a risk of generating multiple structures to allow overfitting of the whole spectral range and one would potentially need to add additional constraints in the fitting.

III. Conclusions

We have applied electrochemically-induced 2D-IR difference spectroscopy on cyt *c* which is one of the most studied redox-active proteins. Despite the extensive investigations undertaken on cyt *c*, the relationship between electron transfer and backbone conformational changes remained unclear, especially because of the apparent inconsistence between the X-ray data where cyt *c* shows no significant secondary structure modifications whereas in solution, IR-spectroscopic data suggest otherwise. The electrochemically-induced FTIR data of cyt *c*

in the amide I range are in line with previous results. The analysis of the redox-induced 2D-IR difference spectrum obtained here is not compatible with previous FTIR assignments because cross-peaks seem to suggest unrealistic couplings between spatially well-separated segments of the protein. Prompted by this discrepancy, we used MD simulations combined with quantum mechanical response function calculations to shed light on the discrepancies between the observed cross-peaks and the literature assignments. We achieved good agreement between the simulated and the experimental FTIR difference spectrum. Our simulation of the 2D-IR spectra did not take into account time dependent effects (i.e. thermalization, relaxation-assisted cross-peaks), and therefore did not allow a direct comparison to the experimental 2D-IR data. However, it helped understanding the complexity of the 2D-IR (difference) spectra.

Importantly, we found that the different segments of the protein contribute in the *entire* amide I spectral range. Surprisingly, we found that the redox-induced change in heme charge creates an amide I spectral response that is as strong or even stronger than the response induced by structural changes. This explains the previously discussed discrepancy between the observation of only subtle structural changes by crystallography and considerable changes in the FTIR spectrum. Moreover,

there are very strong cancellation effects by contributions of the different secondary structure segments in the difference spectrum. According to the computations, the difference spectrum of the whole protein is smaller in signal size than the difference spectra of many of the individual secondary structure segments themselves. Therefore, assigning the FTIR difference spectrum in accordance with previous literature and interpreting the 2D-IR difference spectrum along the same lines led to obvious misinterpretations (i.e. cross-peaks apparently seem to occur between remote sites). This puzzle was solved by MD simulations, which uncovered the severity of cancelation in the difference spectra. Our combination of experiment and theory shows that an unambiguous assignment of a particular spectral feature to a particular structural segment is not possible and the analysis of the rich amide I FTIR and 2D-IR difference spectra of cyt *c* is more complex than previously thought. It is likely that many of our present findings about the complexity of assigning features in FTIR or 2D-IR amide I difference spectra to local structural elements applies for many other protein systems as well, in particular when accompanied by changes in charge.

Supplementary Material

See the supplementary material to access the materials and methods section with all the experimental details as well as the MD simulation parameters. Additional figures and information can also be found.

Acknowledgements

Y. E. K. thanks the Alexander von Humboldt Foundation for a Humboldt Research Fellowship for Postdoctoral Researchers. J. B. thanks the Alexander von Humboldt Foundation for a Sofia Kovalevskaja Award. The authors thank the Deutsche Forschungsgemeinschaft for funding (No. INST 161/722-1 FUGG). We acknowledge Dr. Andreas Roth for building the potentiostat. We thank Viktor Schäfer for support on electronics. This research used resources of the Oak Ridge Leadership Computing Facility at the Oak Ridge National Laboratory, which is supported by the Office of Science of the U.S. Department of Energy under Contract No. DE AC05 00OR22725

Data Availability

The data that support the findings of this study are available from the corresponding author upon reasonable request.

References

[1] Abbreviations: Cyt c, cytochrome c; 2D-IR, two-dimensional infrared; FTIR, Fourier transform infrared; GSB/SE, ground state bleach/stimulated emission; ESA, excited state absorption; Ox, oxidized; Red, reduced; MD, molecular dynamics.
[2] D. Marshall, and P. R. Rich, Methods Enzymol. **456** (2009) 53.
[3] F. Melin, and P. Hellwig, Biol. Chem. **394** (2013) 593.
[4] A. Barth, Biochim. Biophys. Acta. **1767** (2007) 1073.
[5] J. L. R. Arrondo, and F. M. Goni, Prog. Biophys. Mol. Biol. **72** (1999) 367.
[6] Y. Li, Y. Kimura, T. Arikawa, Z. Y. Wang-Otomo, and T. Ohno, Biochemistry **52** (2013) 9001.
[7] A. Marechal, A. M. Hartley, T. P. Warelow, B. Meunier, and P. R. Rich, Biochim. Biophys. Acta Bioenerg. **1859** (2018) 705.
[8] A. Mezzetti, Molecules **20** (2015) 12229.
[9] T. Kottke, V. A. Lorenz-Fonfria, and J. Heberle, J. Phys. Chem. B. **121** (2017) 335.
[10] A. Pfeifer, T. Majerus, K. Zikihara, D. Matsuoka, S. Tokutomi, J. Heberle, and T. Kottke, Biophys. J. **96** (2009) 1462.
[11] A. Mezzetti, M. Alexandre, A. Thurotte, A. Wilson, M. Gwizdala, and D. Kirilovsky, J. Phys. Chem. B. **123** (2019) 3259.
[12] H. S. Chung, Z. Ganim, K. C. Jones, and A. Tokmakoff, Proc. Natl. Acad. Sci. U. S. A. **104** (2007) 14237.
[13] J. Bredenbeck, J. Helbing, A. Sieg, T. Schrader, W. Zinth, C. Renner, R. Behrendt, L. Moroder, J. Wachtveitl, and P. Hamm, Proc. Natl. Acad. Sci. U. S. A. **100** (2003) 6452.
[14] N. Demirdöven, C. M. Cheatum, H. S. Chung, M. Khalil, J. Knoester, and A. Tokmakoff, J. Am. Chem. Soc. **126** (2004) 7981.
[15] Z. Ganim, H. S. Chung, A. W. Smith, L. P. Deflores, K. C. Jones, and A. Tokmakoff, Acc. Chem. Res. **41** (2008) 432.
[16] Y. S. Kim, and R. M. Hochstrasser, J. Phys. Chem. B. **113** (2009) 8231.
[17] S. H. Shim, R. Gupta, Y. L. Ling, D. B. Strasfeld, D. P. Raleigh, and M. T. Zanni, Proc. Natl. Acad. Sci. U. S. A. **106** (2009) 6614.
[18] A. W. Smith, J. Lessing, Z. Ganim, C. S. Peng, A. Tokmakoff, S. Roy, T. L. C. Jansen, and J. Knoester, J. Phys. Chem. B. **114** (2010) 10913.
[19] C. R. Baiz, C. S. Peng, M. E. Reppert, K. C. Jones, and A. Tokmakoff, Analyst **137** (2012) 1793.
[20] P. Hamm, and M. T. Zanni, *Concepts and Methods of 2D Infrared Spectroscopy* (Cambrigde, 2011),
[21] Y. El Khoury, L. J. Van Wilderen, and J. Bredenbeck, J. Chem. Phys. **142** (2015) 212416.
[22] Y. El Khoury, L. J. Van Wilderen, T. Vogt, E. Winter, and J. Bredenbeck, Rev. Sci. Instrum. **86** (2015) 083102.
[23] D. Moss, E. Nabedryk, J. Breton, and W. Mantele, Eur. J. Biochem. **187** (1990) 565.
[24] K. Ataka, and J. Heberle, J. Am. Chem. Soc. **126** (2004) 9445.
[25] A. C. Dong, P. Huang, and W. S. Caughey, Biochemistry **31** (1992) 182.
[26] L. Marboutin, A. Boussac, and C. Berthomieu, J. Biol. Inorg. Chem. **11** (2006) 811.
[27] G. W. Bushnell, G. V. Louie, and G. D. Brayer, J. Mol. Biol. **214** (1990) 585.
[28] Y. P. Ow, D. R. Green, Z. Hao, and T. W. Mak, Nat. Rev. Mol. Cell Biol. **9** (2008) 532.
[29] P. X. Qi, R. A. Beckman, and A. J. Wand, Biochemistry **35** (1996) 12275.
[30] P. X. Qi, D. L. Di Stefano, and A. J. Wand, Biochemistry **33** (1994) 6408.

[31] A. N. Volkov, S. Vanwetswinkel, K. Van de Water, and N. A. van Nuland, J. Biomol. NMR. **52** (2012) 245.
[32] H. Ochi, Y. Hata, N. Tanaka, M. Kakudo, T. Sakurai, S. Aihara, and Y. Morita, J. Mol. Biol. **166** (1983) 407.
[33] M. De March, N. Demitri, R. De Zorzi, A. Casini, C. Gabbiani, A. Guerri, L. Messori, and S. Geremia, J. Inorg. Biochem. **135** (2014) 58.
[34] G. Williams, N. J. Clayden, G. R. Moore, and R. J. Williams, J. Mol. Biol. **183** (1985) 447.
[35] D. D. Schlereth, and W. Mantele, Biochemistry **32** (1993) 1118.
[36] C. Zou, M. Larisika, G. Nagy, J. Srajer, C. Oostenbrink, X. Chen, W. Knoll, B. Liedberg, and C. Nowak, J. Phys. Chem. B. **117** (2013) 9606.
[37] F. S. Husseini, D. Robinson, N. T. Hunt, A. W. Parker, and J. D. Hirst, J. Comput. Chem. **38** (2017) 1362.
[38] M. Reppert, and A. Tokmakoff, Ann. Rev. Phys. Chem. **67** (2016) 359.
[39] A. S. Bondarenko, and T. L. C. Jansen, J. Chem. Phys. **142** (2015) 212437.
[40] A. V. Cunha, A. S. Bondarenko, and T. L. C. Jansen, J. Chem. Theory Comput. **12** (2016) 3982.
[41] M. Ye, Q. L. Zhang, H. Li, Y. X. Weng, W. C. Wang, and X. G. Qiu, Biophys. J. **93** (2007) 2756.
[42] A. C. Dong, P. Huang, and W. S. Caughey, Arch. Biochem. Biophys. **320** (1995) 59.
[43] J. Kubelka, and T. A. Keiderling, J. Am. Chem. Soc. **123** (2001) 12048.
[44] S. Venyaminov, and N. N. Kalnin, Biopolymers **30** (1990) 1259.
[45] J. Bandekar, and S. Krimm, Proc. Natl. Acad. Sci. U. S. A. **76** (1979) 774.
[46] A. Barth, and C. Zscherp, Q. Rev. Biophys. **35** (2002) 369.
[47] E. H. Backus, P. H. Nguyen, V. Botan, R. Pfister, A. Moretto, M. Crisma, C. Toniolo, G. Stock, and P. Hamm, J Phys Chem B **112** (2008) 9091.
[48] L. Valino Borau, A. Gulzar, and G. Stock, J Chem Phys **152** (2020) 045103.
[49] A. S. Bondarenko, I. Patmanidis, R. Alessandri, P. C. T. Souza, T. L. C. Jansen, A. H. de Vries, S. J. Marrink, and J. Knoester, Chem. Sci. **11** (2020) 11514.
[50] A. S. Sardjan, F. P. Westerman, J. P. Ogilvie, and T. L. C. Jansen, J. Phys. Chem. B. **124** (2020) 9420.
[51] L. Wang, C. T. Middleton, S. Singh, A. S. Reddy, A. M. Woys, D. B. Strasfeld, P. Marek, D. P. Raleigh, J. J. de Pablo, M. T. Zanni, and J. L. Skinner, J. Am. Chem. Soc. **133** (2011) 16062.
[52] L. P. Deflores, Z. Ganim, R. A. Nicodemus, and A. Tokmakoff, J. Am. Chem. Soc. **131** (2009) 3385.
[53] S. Hume, G. Hithell, G. M. Greetham, P. M. Donaldson, M. Towrie, A. W. Parker, M. J. Baker, and N. T. Hunt, Chem. Sci. **10** (2019) 6448.
[54] D. B. Strasfeld, Y. L. Ling, S. H. Shim, and M. T. Zanni, J. Am. Chem. Soc. **130** (2008) 6698.
[55] X.-X. Zhang, K. C. Jones, A. Fitzpatrick, C. S. Peng, C.-J. Feng, C. R. Baiz, and A. Tokmakoff, J. Phys. Chem. B. **120** (2016) 5134.
[56] M. Grechko, and M. T. Zanni, J. Chem. Phys. **137** (2012)
[57] P. Hamm, M. H. Lim, and R. M. Hochstrasser, J. Phys. Chem. B. **102** (1998) 6123.
[58] P. L. McRobbie, G. Hanna, Q. Shi, and E. Geva, Acc. Chem. Res. **42** (2009) 1299.
[59] C. P. van der Vegte, S. Knop, P. Vohringer, J. Knoester, and T. L. C. Jansen, J. Phys. Chem. B. **118** (2014) 6256.
[60] D. V. Kurochkin, S. R. Naraharisetty, and I. V. Rubtsov, Proc. Natl. Acad. Sci. U. S. A. **104** (2007) 14209.
[61] I. V. Rubtsov, Acc. Chem. Res. **42** (2009) 1385.
[62] S. Woutersen, and P. Hamm, J. Chem. Phys. **114** (2001) 2727.

[63] S. D. Moran, A. M. Woys, L. E. Buchanan, E. Bixby, S. M. Decatur, and M. T. Zanni, Proc. Natl. Acad. Sci. U. S. A. **109** (2012) 3329.
[64] S. Roy, T. L. C. Jansen, and J. Knoester, Phys. Chem. Chem. Phys. **12** (2010) 9347.
[65] J. Lessing, S. Roy, M. Reppert, M. Baer, D. Marx, T. L. C. Jansen, J. Knoester, and A. Tokmakoff, J. Am. Chem. Soc. **134** (2012) 5032.
[66] O. Selig, A. V. Cunha, M. B. van Eldijk, J. C. M. van Hest, T. L. C. Jansen, H. J. Bakker, and Y. L. A. Rezus, J. Phys. Chem. B. **122** (2018) 8243.
[67] H. T. Kratochvil, J. K. Carr, K. Matulef, A. W. Annen, H. Li, M. Maj, J. Ostmeyer, A. L. Serrano, H. Raghuraman, S. D. Moran, J. L. Skinner, E. Perozo, B. Roux, F. I. Valiyaveetil, and M. T. Zanni, Science **353** (2016) 1040.
[68] W. Kopec, D. A. Kopfer, O. N. Vickery, A. S. Bondarenko, T. L. C. Jansen, B. L. de Groot, and U. Zachariae, Nat. Chem. **10** (2018) 813.
[69] M. Maj, J. P. Lomont, K. L. Rich, A. M. Alperstein, and M. T. Zanni, Chem. Sci. **9** (2018) 463.
[70] M. M. Waegele, R. M. Culik, and F. Gai, J. Phys. Chem. Lett. **2** (2011) 2598.
[71] S. Ramos, and M. C. Thielges, J. Phys. Chem. B. **123** (2019) 3551.
[72] R. Adhikary, J. Zimmermann, and F. E. Romesberg, Chem. Rev. **117** (2017) 1927.
[73] C. R. Hall, J. Tolentino Collado, J. N. Iuliano, K. Adamczyk, A. Lukacs, G. M. Greetham, I. V. Sazanovich, P. J. Tonge, and S. R. Meech, J. Phys. Chem. B. (2019)
[74] L. Blankenburg, L. Schroeder, F. Habenstein, B. Błasiak, T. Kottke, and J. Bredenbeck, Phys. Chem. Chem. Phys. **21** (2019) 6622.
[75] L. J. G. W. van Wilderen, H. Brunst, H. Gustmann, J. Wachtveitl, J. Broos, and J. Bredenbeck, Phys. Chem. Chem. Phys. **20** (2018) 19906.
[76] L. J. van Wilderen, D. Kern-Michler, H. M. Muller-Werkmeister, and J. Bredenbeck, Phys. Chem. Chem. Phys. **16** (2014) 19643.
[77] L. J. G. W. van Wilderen, D. Kern-Michler, H. M. Müller-Werkmeister, and J. Bredenbeck, Phys. Chem. Chem. Phys. **19** (2017) 9676.
[78] J. M. Schmidt-Engler, L. Blankenburg, B. Błasiak, L. J. G. W. van Wilderen, M. Cho, and J. Bredenbeck, Anal. Chem. **92** (2020) 1024.
[79] S. Hu, K. M. Smith, and T. G. Spiro, J. Am. Chem. Soc. **118** (1996) 12638.
[80] S. Hu, I. K. Morris, J. P. Singh, K. M. Smith, and T. G. Spiro, J. Am. Chem. Soc. **115** (1993) 12446.
[81] W. A. Kalsbeck, A. Ghosh, R. K. Pandey, K. M. Smith, and D. F. Bocian, J. Am. Chem. Soc. **117** (1995) 10959.
[82] Y. Sugita, and Y. Okamoto, Chem. Phys. Lett. **314** (1999) 141.

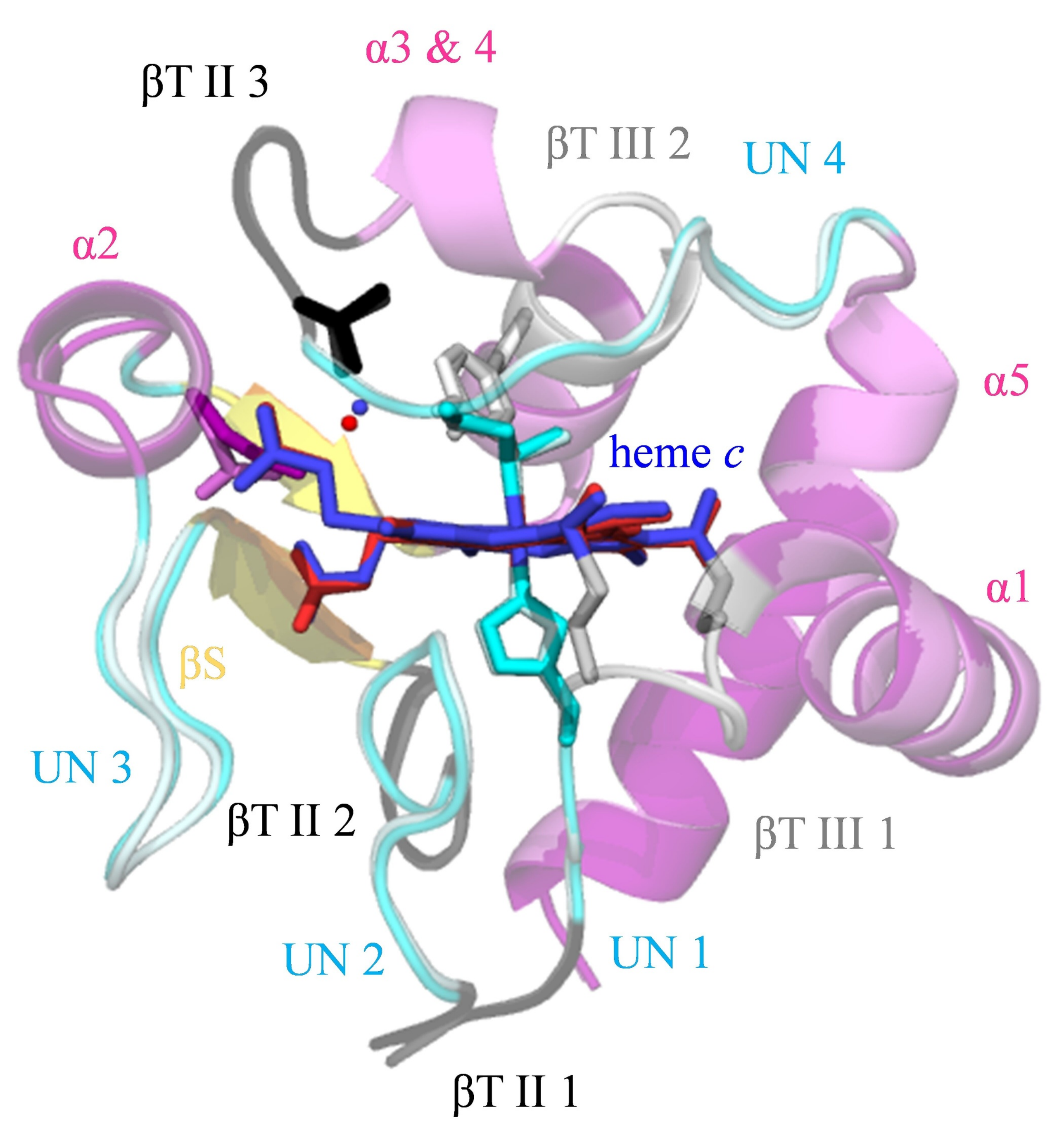
βT II 3
α3 & 4
βT III 2
UN 4
α2
α5
heme c
α1
βS
UN 3
βT II 2
βT III 1
UN 2
UN 1
βT II 1

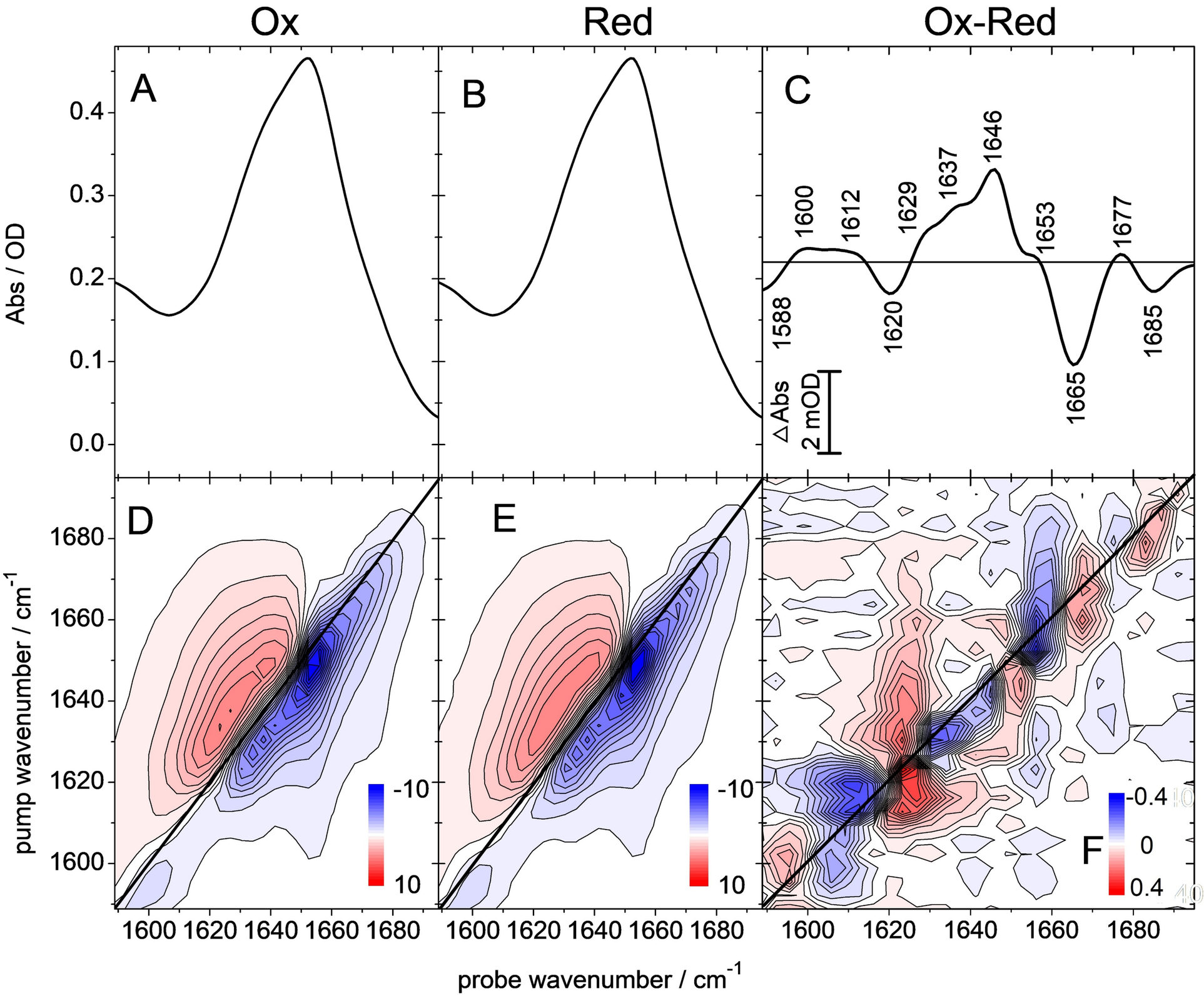
Ox
Red
Ox-Red
A
B
C
D
E
F
Abs / OD
0.0
0.1
0.2
0.3
0.4
1600
1612
1629
1637
1646
1653
1677
1588
1620
1665
1685
ΔAbs
2 mOD
pump wavenumber / cm-1
1600
1620
1640
1660
1680
-10
10
-0.4
0
0.4
probe wavenumber / cm-1

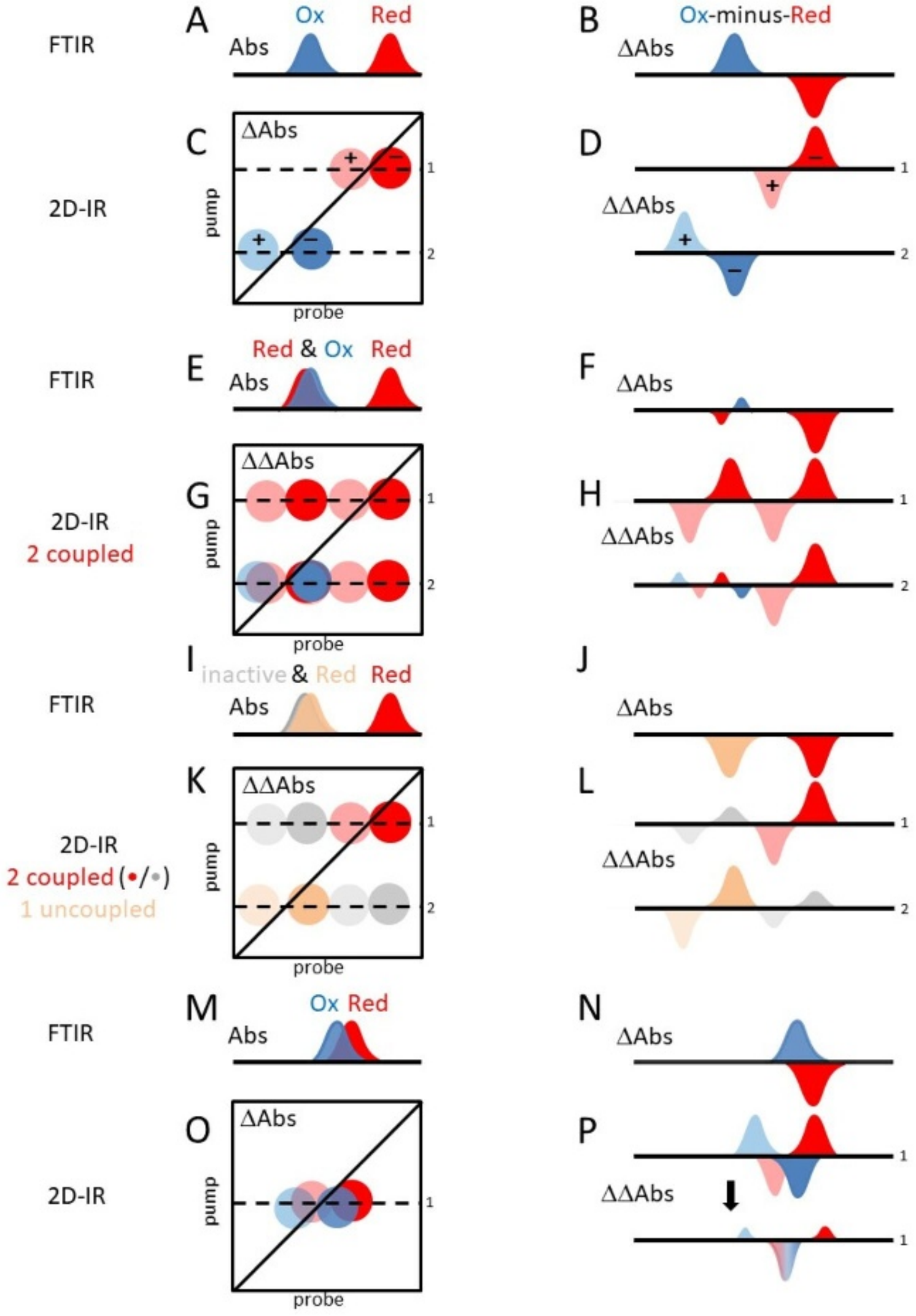
FTIR
A
Ox
Red
Abs
B
Ox-minus-Red
ΔAbs
2D-IR
C
ΔAbs
pump
probe
1
2
D
ΔΔAbs
FTIR
E
Red & Ox Red
Abs
F
ΔAbs
2D-IR
2 coupled
G
ΔΔAbs
H
ΔΔAbs
FTIR
I
inactive & Red Red
Abs
J
ΔAbs
2D-IR
2 coupled (•/•)
1 uncoupled
K
ΔΔAbs
L
ΔΔAbs
FTIR
M
Ox Red
Abs
N
ΔAbs
2D-IR
O
ΔAbs
P
ΔΔAbs

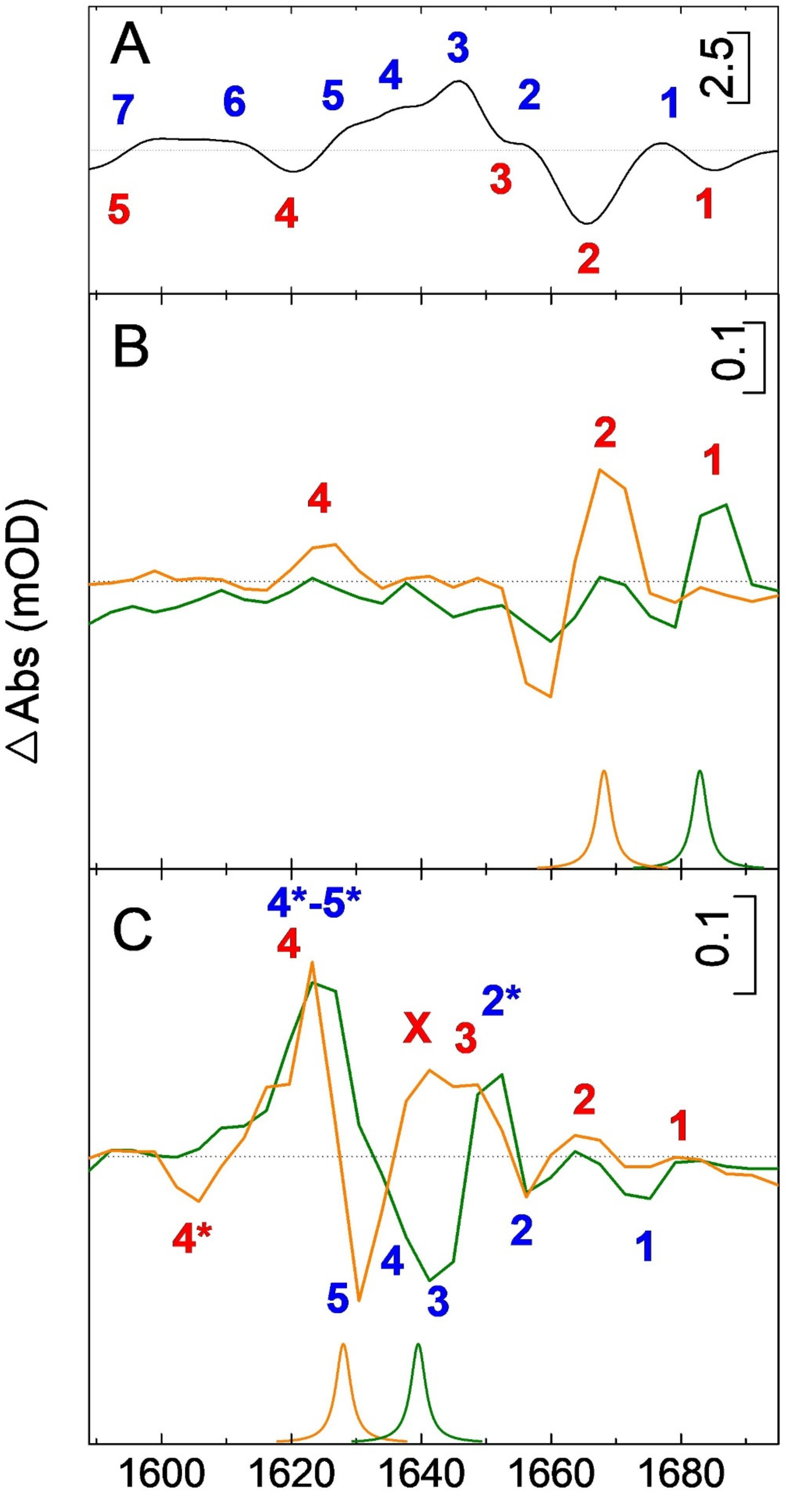
A
7
6
5
4
3
2
1
2.5
5
4
3
2
1
B
0.1
4
2
1
C
4*-5*
4
0.1
X
3
2*
2
1
4*
5
4
3
2
1
1600
1620
1640
1660
1680
probe wavenumber / cm-1
ΔAbs (mOD)

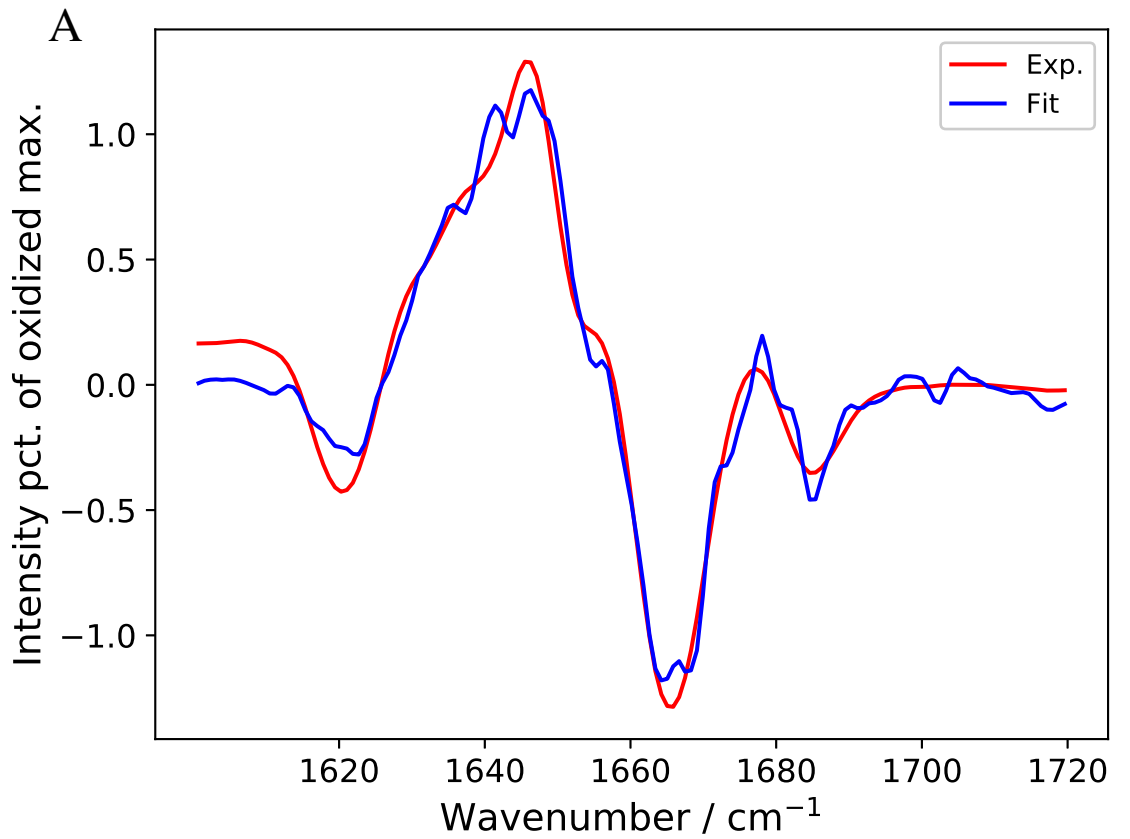
A
Exp.
Fit
1.0
0.5
0.0
−0.5
−1.0
Intensity pct. of oxidized max.
1620
1640
1660
1680
1700
1720
Wavenumber / cm^{-1}

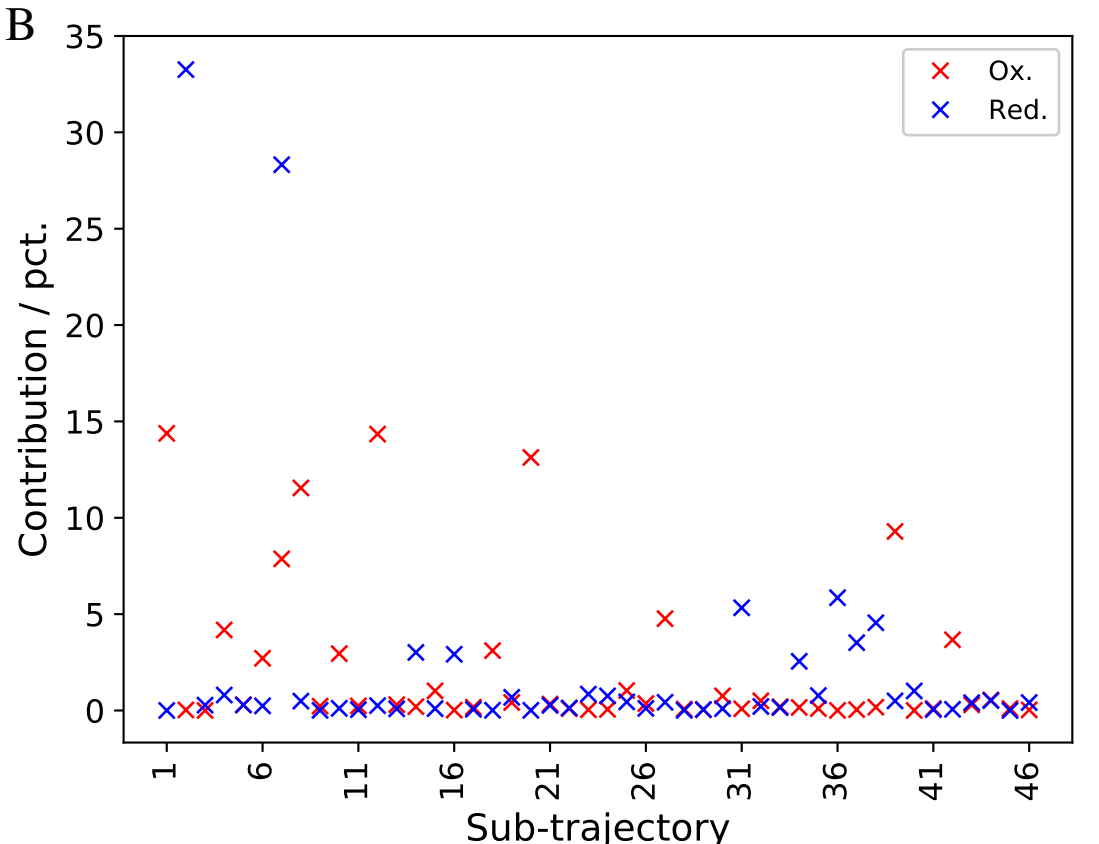
B
Ox.
Red.
35
30
25
20
15
10
5
0
Contribution / pct.
1
6
11
16
21
26
31
36
41
46
Sub-trajectory

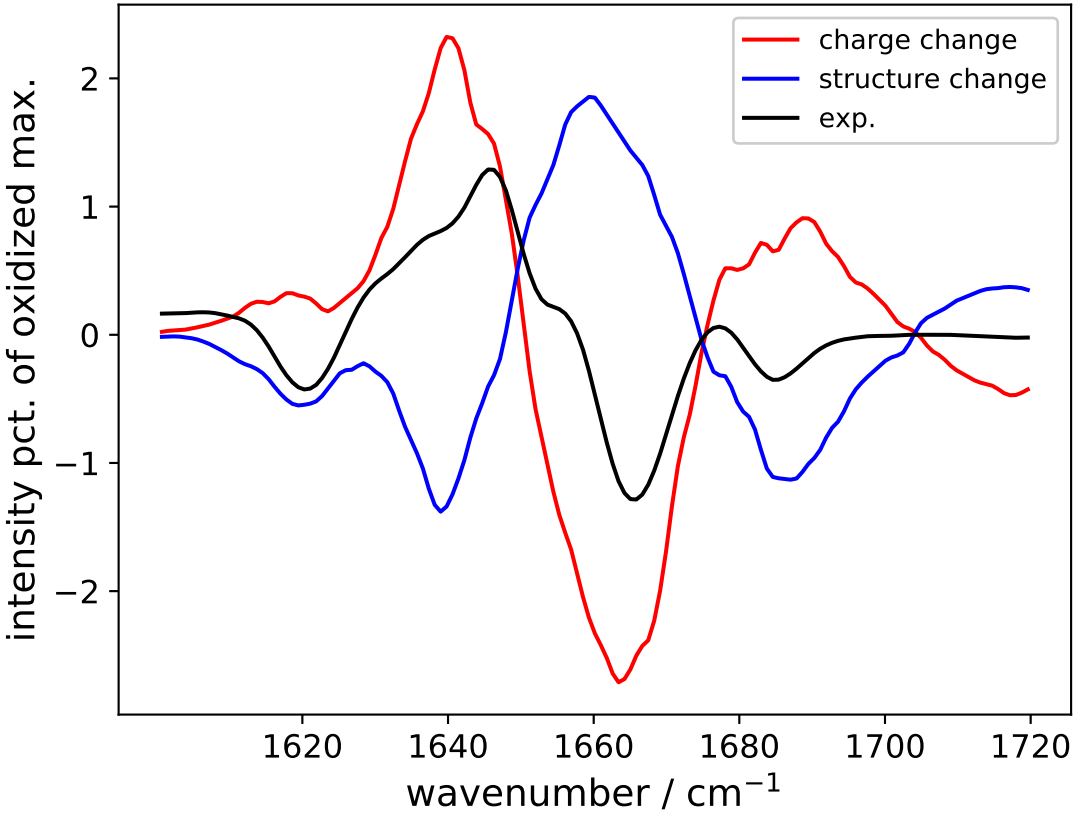
charge change
structure change
exp.
intensity pct. of oxidized max.
2
1
0
−1
−2
1620
1640
1660
1680
1700
1720
wavenumber / cm^{-1}

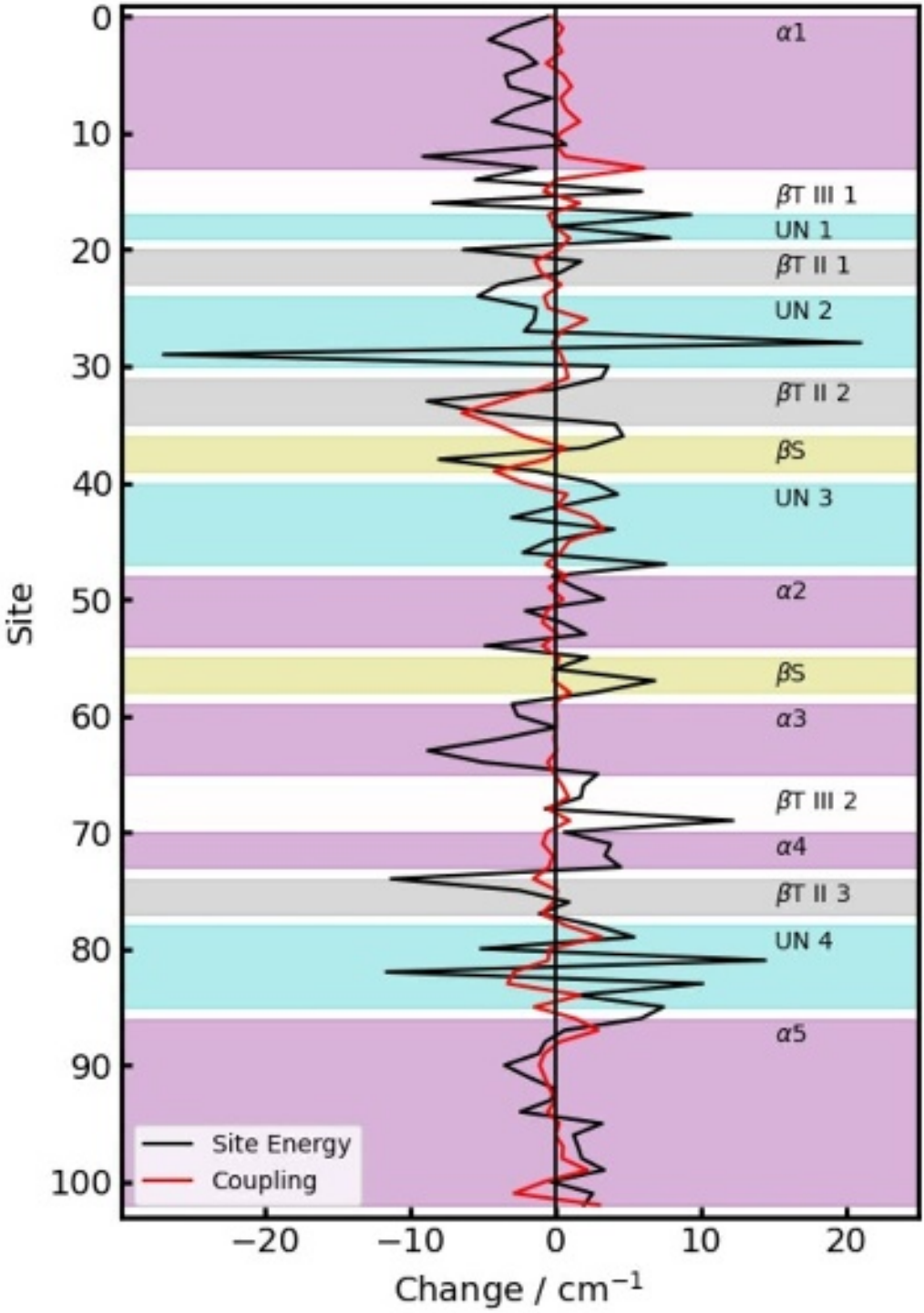
Site
0
10
20
30
40
50
60
70
80
90
100
α1
βT III 1
UN 1
βT II 1
UN 2
βT II 2
βS
UN 3
α2
βS
α3
βT III 2
α4
βT II 3
UN 4
α5
Site Energy
Coupling
−20
−10
0
10
20
Change / cm^{-1}

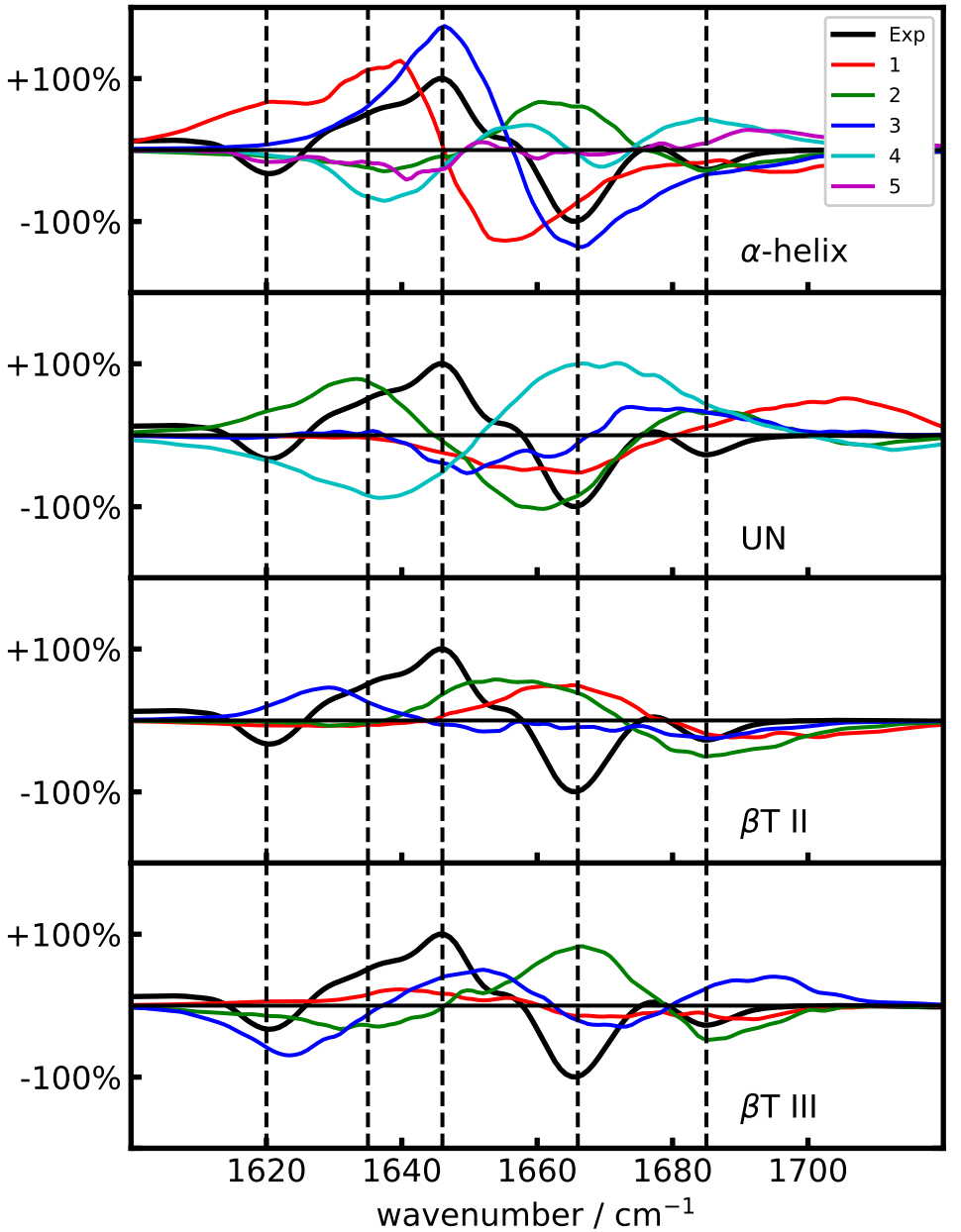
Exp
1
2
3
4
5
+100%
-100%
α-helix
+100%
-100%
UN
+100%
-100%
βT II
+100%
-100%
βT III
1620
1640
1660
1680
1700
wavenumber / cm^{-1}

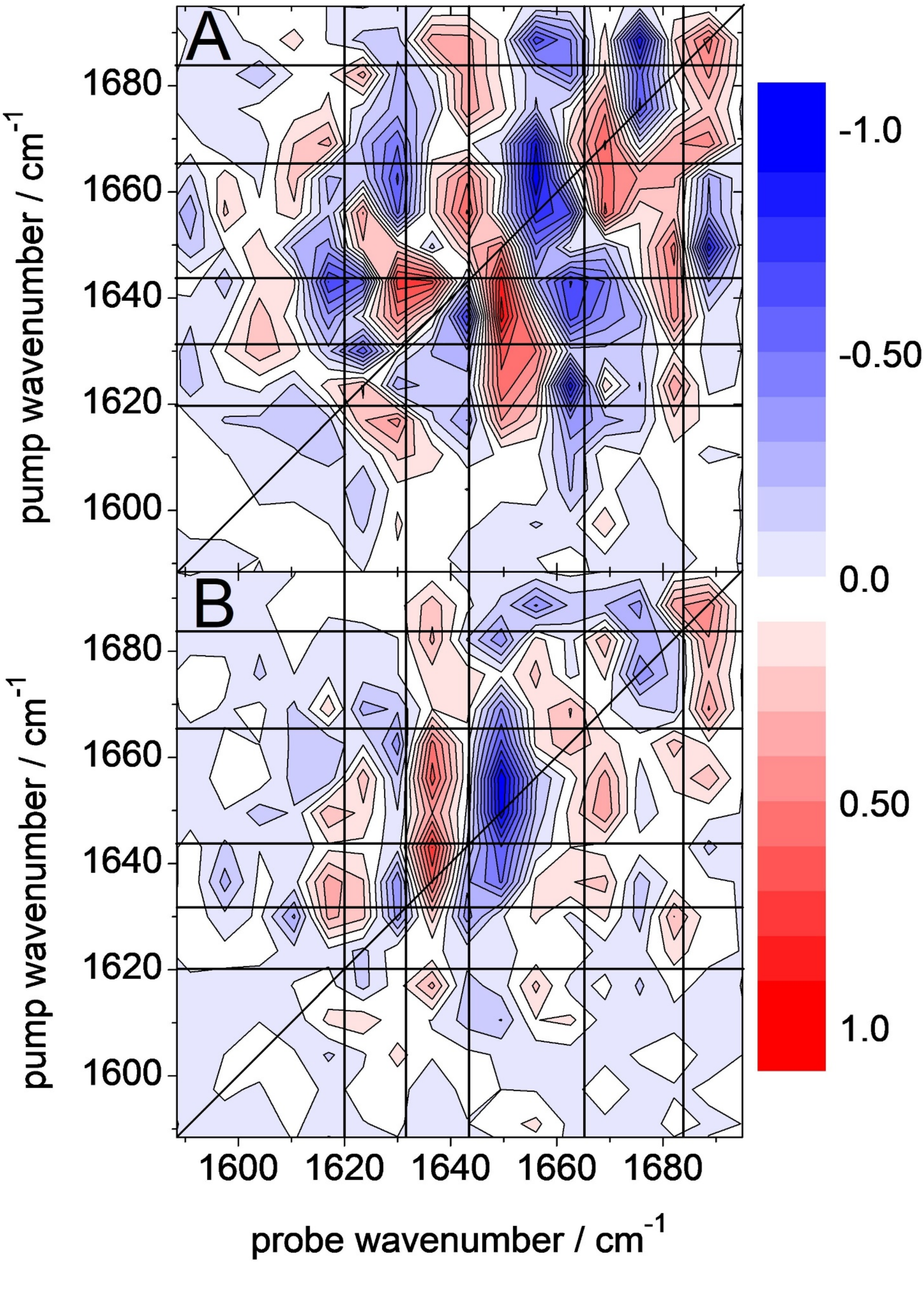
A
B
1680
1660
1640
1620
1600
pump wavenumber / cm-1
1600
1620
1640
1660
1680
probe wavenumber / cm-1
-1.0
-0.50
0.0
0.50
1.0